Journal of Emergency Medicine and Care
Volume 1 | Issue 2

Review Article Open Access

Oxygen Balance Homeostasis and Tissue Metabolic Score (TMS) of Patients in Emergency and Critical Care Medicine

Mayevsky A*, Tolmasov M, Kutai-Asis H and Mandelbaum M

The Mina & Everard Goodman Faculty of Life Sciences, Bar-Ilan University, Ramat-Gan 5290092, Israel

***Corresponding author:** Avraham Mayevsky, PhD, Professor Emeritus, The Mina & Everard Goodman Faculty of Life Sciences, Bar-Ilan University, Ramat-Gan 5290002, Israel, Fax: 972-3-5351561, Tel: 972-544-861854, E-mail: mayevskya@gmail.com

Citation: Mayevsky A, Tolmasov M, Kutai-Asis H, Mandelbaum M (2018) Oxygen Balance Homeostasis and Tissue Metabolic Score (TMS) of Patients in Emergency and Critical Care Medicine. J Emerg Med Care 1(2): 204

Received Date: September 14, 2018 **Accepted Date:** December 29, 2018 **Published Date:** December 31, 2018

Abstract

Patients admitted to the emergency room or intensive care units (ICUs) need real time monitoring of body oxygen balance. As of today the availability of monitoring devices that provide real time data on tissue level of oxygen homeostasis is very limited. The involvement of mitochondrial dysfunction in many pathological states such as stroke, sepsis or heart failure is calling for real time evaluation of this intracellular organelle. In order to avoid the deterioration of the most vital organs in the body (brain and heart) we are proposing to monitor a less vital organ, such as the urethral wall, that serves as an early warning signal for the deterioration of body oxygen balance. This review describes the use of a multiparametric monitoring device (CritiView) connected to the patient's urethral wall via a 3-way Foley catheter that measures in real time 4 parameters representing tissue oxygen balance. Mitochondrial NADH is measured by surface fluorometry/reflectometry. In addition, tissue microcirculatory blood flow, tissue reflectance and hemoglobin oxygenation are measured as well. The measured 4 parameters could be integrated together with systemic hemodynamic parameters to provide in real time a new Tissue Metabolic Score (TMS). The device was tested both *in vitro* and *in vivo* in a small animal models (rats and gerbils) exposed to changes in local or systemic oxygen balance. Also preliminary clinical trials in patients undergoing vascular or open heart surgery were performed. In patients, the monitoring started immediately after the insertion of a 3-way Foley catheter (urine collection) to the patient and was stopped when the patient was discharged from the operation room. The results show that monitoring the Urethral wall oxygen balance provides real time information correlated to the state of the surgical procedure performed. We found that the TMS of the urethral wall could serve as an early warning signal for the possible damage that may develop in the most vital organs in the body.

Keywords: Mitochondrial NADH; Microcirculation; NADH Redox State; Microcirculatory Hemoglobin Oxygenation; Multiparametric Monitoring; Hemorrhagic Shock; Blood Flow Redistribution; Early Warning Signal

Introduction

About 150 years ago the French physiologist Claude Bernard coined the concept "Millieu Interieur" that described the stability of the internal environment enabling the free and independent life of multicellular organisms. Later on, the American physiologist Walter Bradford Canon coined the term "fight or flight response" and expanded on the Claude Bernard's concept of homeostasis. This autoregulation mechanism enables the multicellular organism to keep various key physiological parameters in a relatively narrow range. It includes fluid balance, temperature, pH of extracellular fluid, concentration of various ions as well as blood sugar. The regulation of adequate oxygen supply is a crucial factor that enables the organism to avoid the development of pathological conditions that may lead to irreversible damage.

In the present review, the homeostasis of oxygen balance will be discussed in patients exposed to various emergency and critical care conditions.

Cellular Energy Metabolism

All cells in the body depend on a continuous supply of ATP (adenosine tri-phosphate) in order to perform their different physiological and biochemical activities. Figure 1 describes the basic processes occurring in a typical normal cell, using glucose as a major source of energy. The source of oxygen for mitochondrial function is the microcirculation as shown in the left side of Figure 1.

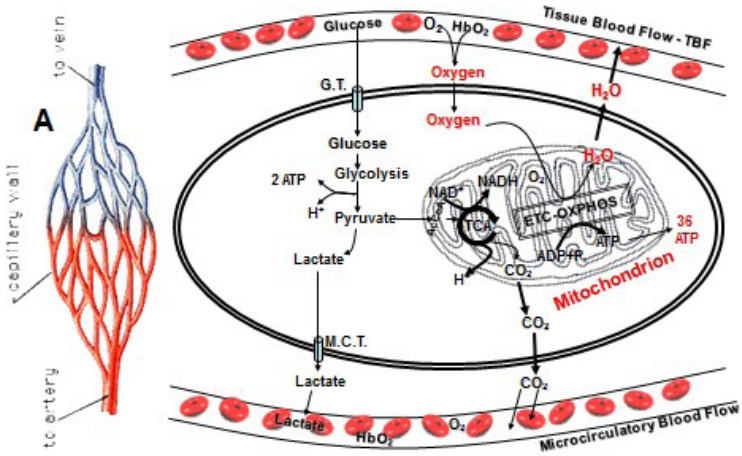

Figure 1: Schematic presentation of tissue oxygen metabolism at the cellular and intramitochondrial level. A - The supply of oxygen via the microcirculation. G.T. - Glucose Transporter, M.C.T. –Monocarboxylase Transporter, ETC – Electron transport chain, OXPHOS - Oxidative phosphorylation, TCA - Tricarboxylic acid cycle.

The breakdown of glucose into water and CO_2 includes two steps, namely, glycolysis (the anaerobic phase) taking place in the cytoplasm, and oxidative phosphorylation (the aerobic phase) occurring in the mitochondria. Of the total yield of 38 ATP per mole of glucose, 2 are produced in the glycolysis process and 36 during the oxidative phosphorylation. It is important to note that oxygen availability in the mitochondrion is a critical factor for the normal ATP production in the cell. The exact level of oxygen inside the mitochondria *in vivo* is not well defined due to the inaccuracy of the measurement tools. It is evaluated to be around 1mm Hg as compared to the high partial oxygen pressure, around 90 mmHg, existing in systemic circulation [1]. Glycolysis depends on the entrance of glucose from the capillary into the cell via the glucose transporter. The end product of glycolysis, pyruvate, is transported into the mitochondria by a specific carrier protein. The pyruvate is transformed, in the matrix of the mitochondria, into acetyl Coenzyme A that activates the tricarboxylic acid (TCA) cycle. In the absence of oxygen, the end product of pyruvate is lactate that may leave the cell and pass into the microcirculatory blood stream via the monocarboxylase transporter located in the plasma membrane. In the mitochondria, the TCA cycle generates NADH (reduced Nicotineamide Adenine Dinucleotide) which enters the electron transport chain (ETC) leading to the oxidative phosphorylation that generates ATP. The CO_2 released from the TCA cycle exit the cell as HCO_3^-, via the anion exchanger, into the blood stream. The continuous supply of oxygen to the mitochondria depends on two microcirculatory parameters: tissue blood flow (TBF) in the diffusible small vessels (small arterioles and capillaries), and the level of hemoglobin oxygenation or saturation (HbO_2) in the small vessels. Any change in the oxygen consumption by the mitochondria will be compensated either by downloading the extra oxygen needed from oxygenated hemoglobin or via an increase in the blood flow. Under a restriction of oxygen supply (hypoxia or ischemia), mitochondrial function will be inhibited and ATP production will decrease, while glycolysis will become stimulated. In most normal tissues and organs, this stimulation is not sufficient to provide the amount of ATP needed for the normal physiological and biochemical activities.

The Mitochondrion

The discovery of mitochondria in general came in 1890 when Richard Altmann, a cytologist, identified the organelles and dubbed them “bioblasts" [2]. Carl Benda, in 1898, coined the term mitochondria from Greek thread, mitos, and granule, chondros [3].

Disturbances of mitochondrial function lead to disruption of cellular activities, inducing various human pathogeneses such as neurodegenerative processes, apoptotic and aging processes. Moreover, mitochondrial dysfunction is involved in the pathologies of the nervous system, such as traumatic brain injury and stroke [4]. The mitochondria, as an energy production system, are involved in tumor cell pathogenesis, initially described by Warburg 80 years ago and later followed by many studies [5,6]. The role of NADH in cellular function and cell death as well as in brain functions, diseases and aging were reviewed [7]. In 2013 Edeas and Weissig published a paper claiming that the future of medicine will come through mitochondria [8]. The discovery of the pyridine nucleotides was made by Harden & Young about 110 years ago and was followed by the description of their full structure by Warburg and collaborators 30 years later [9,10]. All those historical studies led to the first detailed experiments, by Chance *et al.*, in which NADH was used as a marker of mitochondrial function of the brain and kidney *in vivo* in the anesthetized rats [11]. The optical properties of NADH have led to a very intensive research since the early 1950's. Only the reduced form of this molecule, NADH, absorbs light at 320-380 nm (Figure 2A and B) and emits fluorescent light at 420-480 nm range (Figure 2C) [4,12]. Therefore, when a mixture of NADH and NAD+ is illuminated in a cuvette by 320-380 nm, only NADH will affect the absorption spectrum peak at 340 nm. The absorption and fluorescence spectra of NADH (the reduced form) have been well characterized at different levels of organization, i.e., in solution, mitochondria and cell suspensions, tissue slices, and organs *in vitro* and *in vivo.*

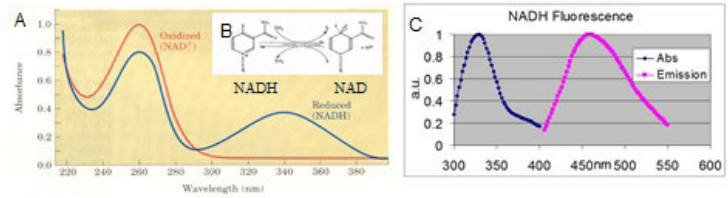

D

TABLE 2 - Metabolic States of Mitochondria and Associated Oxidation-Reduction Levels of Respiratory Enzymes

State	$[O_2]$	ADP level	Substrate level	Respiration rate	Rate-limiting substance	Steady state percentage reduction of components: a	c	b	Flavoprotein[a]	$NADH_1$
1	>0	Low	Low	Slow	ADP	0	7	17	21	~90
2	>0	High	~0	Slow	Substrate	0	0	0	0	0
3	>0	High	High	Fast	Respiratory chain	4	6	16	20	53
4	>0	Low	High	Slow	ADP	0	14	35	40	99
5	0	High	High	0	Oxygen	~100	~100	~100	~100	~100

[a] These values are based on the amount of flavoprotein of the respiratory chain. Other fractions, reduced by anoxia, are present but disregarded here.
Source: After Chance and Williams [13].

Figure 2: A - Absorption Spectra of NAD+ (red) and NADH (blue). The transition between oxidized and reduced NADH is in the insert B. C - Excitation and NADH fluorescence emission spectra. D - The classical table of Chance and Williams (1955) describing the various metabolic states of the isolated mitochondria. The changes in the redox state of the various respiratory chain enzymes appear in the right side.

However, there is a universal agreement that the intensity of the fluorescence band, independent of the organization level of the environment, is proportional to the concentration of mitochondrial NADH (the reduced form), particularly when measured *in vivo* from a tissue.

A definitive description of the mitochondrial metabolic state has never been given for *in vivo* conditions. Therefore, we described the *in vivo* mitochondria conditions as recorded by NADH fluorescence in a representative tissue or organ – e.g. the brain. While the range between minimal NADH (~0) and its maximal level was determined *in vitro,* it is almost impossible to determine in the intact brain or other organs *in vivo*. For example, State 2, with a substrate free medium, could not be achieved *in vivo* since the tissue would die. On the other hand, the maximal level of NADH (State 5) could be monitored *in vivo* under complete deprivation of oxygen by anoxia or complete ischemia. We used the changes in NADH levels monitored *in vivo* to create a new scale ranging from a maximal definite point to the minimal level as shown in (Figure 1B). Details of this approach have been published [13].

The biochemical and physiological significance of these spectral qualities is also universally accepted, that is, an increase in the fluorescence intensity indicates a more reduced state of NADH and of the rest of the mitochondrial electron transfer chain. Under various circumstances, changes in the redox state of the electron transport chain can be associated with various conditions. In figure 2D, the metabolic states of the mitochondria *in vitro* defined by Chance and Williams are shown [14]. The "resting" state of the mitochondria *in vitro* was defined as "State 4", where NADH was 99% in the reduced form, and ADP was the rate limiting substance. If ADP is added to a suspension of mitochondria, ATP synthesis will be stimulated, oxygen consumption will increase and the rate limit will be determined by the activity of the respiratory chain. During this State 3, or the "active state," the NADH redox state will decrease or become more oxidized (about 50%). When the "resting" mitochondria are deprived of oxygen, the activity of the mitochondria will stop and NADH will reach its maximum redox state (State 5).

Oxygen Balance Homeostasis

Barcroft J (1914) The Respiratory Function of Blood. Cambridge University Press, Cambridge.

Chapter XI: THE CALL FOR OXYGEN BY THE TISSUES

Page 73: The classical work of Pflüger (1) on the combustion of living material settled for all time, it seems to me, the logical order in which the constituent processes of respiration should be treated.
The issue before Pflüger may be stated in a few words. Is the quantity of oxygen taken up by the cell conditioned primarily by the needs of the cell, or by the supply of oxygen ? The answer was clear, the cell takes what it needs and leaves the rest.

The present chapter will deal with the following theme: **"There is no instance in which it can be proved that an organ increases its activity, under physiological conditions, without also increasing its demand for oxygen."**

Page 105: In our discussion of the call for oxygen we have reviewed the activity of many organs of the body, muscle, heart, kidney, secreting glands and absorbing epithelium; these organs are excited by the most diverse forms of stimulus, electrical stimuli, hormones, drugs, etc. and evidence their activity by doing work of the most diverse kinds; in one respect only do they resemble one another, namely **that in no organ excited by any form of stimulus can it be shown that positive work is done without the blood supply having to respond to a call for oxygen.**

(1) Pflüger, "Ueber die physiologische Verbrennung in den lebendigen Organismen," Pflüger's Arch, x, p. 350, 1875.

Figure 3: Citations from the book published in 1914 by Barcroft regarding the call for oxygen by tissues at rest or during activation

The functional capacity of any tissue is related to its ability to perform its work. It is possible to assess this ability through the knowledge of changes in the oxygen balance, i.e. the ratio of oxygen supply to oxygen demand in the tissue. This concept was suggested by Barcroft more than 100 years ago, as seen in Figure 3 [15]. He described the relationship between tissue activity, oxygen consumption and increase in blood supply as a compensation mechanism. This observation that was published in 1914 has been widely supported by many studies published in the past 100 years. The development of many techniques in physiological monitoring of tissues *in vivo* enabled the researchers to demonstrate Barcroft's concept in many experimental models.

Schematic presentation of the balance between oxygen supply and demand in a typical tissue is shown in Figure 4. The supply of oxygen is dependent upon tissue microcirculatory blood flow (TBF), blood volume and the level of oxygen bound to the hemoglobin (HbO_2) in the small blood vessels. The level of oxygenated hemoglobin in the microcirculation is affected by two factors, namely, oxygen consumption by the mitochondria and the microcirculatory blood flow. The demand for oxygen is affected by the specific activities taking place in each organ as seen in the right side of Figure 4. The intracellular level of mitochondrial NADH (the reduced form) is a parameter related to oxygen balance. Figure 5 shows the gradient of oxygen between room air through the lungs, heart, large arteries and small arterioles to the intracellular space and finally the mitochondrion. In this scheme the various points of patients' monitoring are presented. Since the delivery of oxygen is done mainly in the microcirculation, the level of oxygen in the large arteries is still very high (100 mmHg). As can be seen, the last common parameter, in the oxygen gradient, that is monitored clinically is the pulse oximeter that measures the saturation of hemoglobin in the large arteries. At this point, the hemoglobin is highly saturated as seen in point 1, part A of the figure. The saturation of the hemoglobin at the microcirculation depends on the organ that is monitored. In active organs, such as the brain, heart or kidney, the saturation will be at the levels below 50% and in the resting muscle it will be around 80%. As of today, the monitoring of microcirculation and especially mitochondrial function is not a standard approach and has not become a clinical tool for daily medical practice.

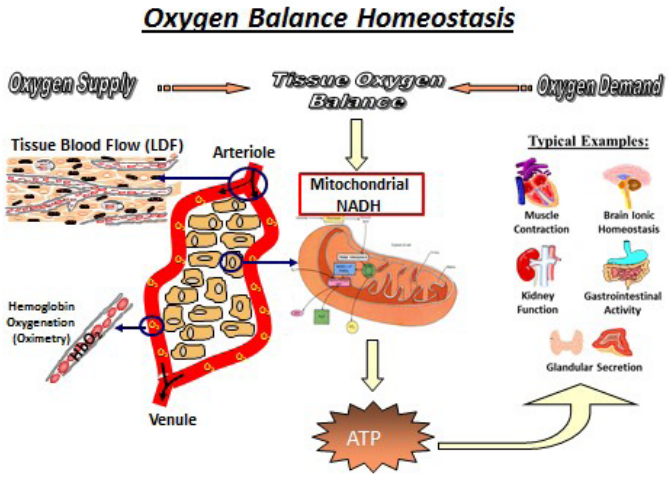

Figure 4: Schematic presentation of tissue oxygen balance evaluated by energy supply and demand. Energy supply could be measured by monitoring tissue blood flow (TBF), tissue blood volume (TBV) and hemoglobin oxygenation (HbO_2) which is similar in all tissues. Energy demand varies between the different tissues and may include Ionic Homeostasis and Signal Conduction (brain), Muscle contraction (heart), Glandular Secretion, G-I tract and kidney function. Mitochondrial NADH redox state serves as an indicator for tissue oxygen balance.

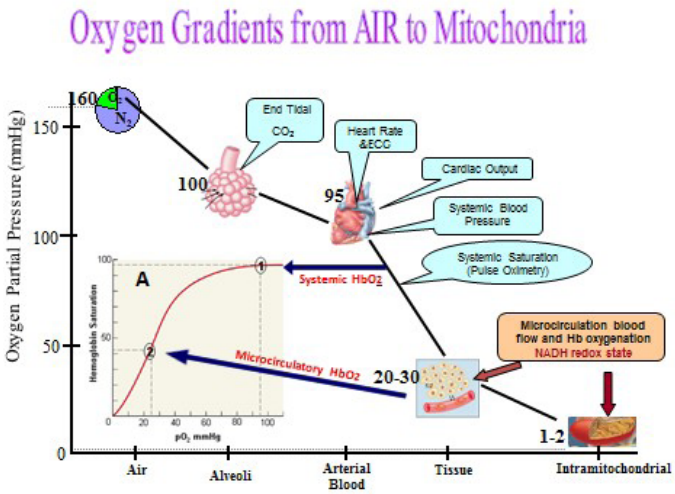

Figure 5: Oxygen gradient from air via the respiratory and cardiovascular systems to the mitochondria. Clinical monitoring of patients includes the various parameters shown along the oxygen gradient. Insert A shows the dissociation curve of oxygen from hemoglobin.

The detailed description of the possible monitored parameters along the oxygen gradient scheme, shown in Figure 5, is described in Figure 6. The first row presents the compartments that are the main points in the oxygen gradient map. The partial pressure of oxygen (pO_2) levels is shown in the second row. The available techniques that could be used to monitor various parameters along the oxygen gradient curve are shown in the left row. The first group of parameters represents the systemic vital signs, routinely measured in patients treated in operating rooms (ORs), ICUs and emergency departments. The 2nd group of parameters representing the microcirculation is available for measurement, but not commonly used in patients. The last parameter that represents the tissue oxygen homeostasis – the mitochondrial redox state – is the most important parameter, but it has not yet been used in clinical practice.

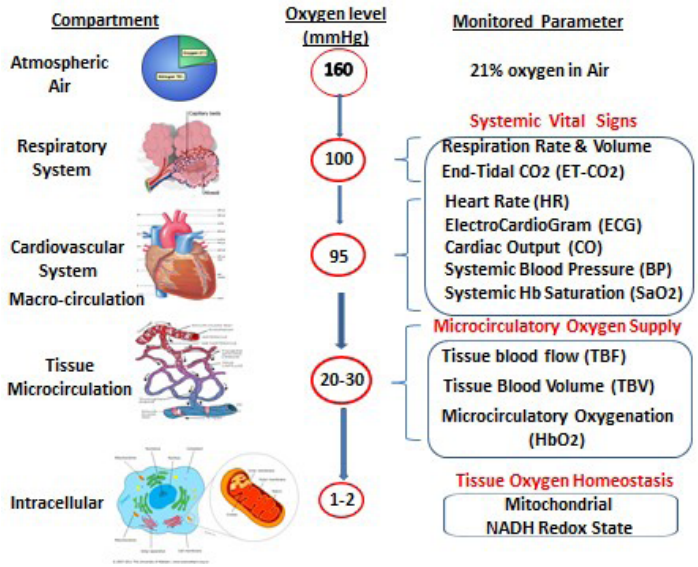

Figure 6: The possible monitored parameters related to oxygen supply and demand from air to the mitochondria.

Monitoring of Patients in Critical Care - Introduction

The monitoring of patients in critical care and in real time could be divided into 2 possible categories as shown in Figure 7. In part A, when a specific organ is monitored, the accumulated information represents the events occurring in the organ itself. For example, monitoring the intra-cranial pressure (ICP) or the Electroencephalography (EEG) in neurosurgical patients will provide information about the events developing in the brain itself [16]. The information depends initially upon local pathological events occurring in the brain. Monitoring Electrocardiography (ECG) represents the electrical activity of the heart, and most of the changes are initially correlated to local and not systemic events. In tissue regeneration or organ transplantation, the monitored parameters, such as microcirculatory blood flow or mitochondrial function, will represent the quality of the tissue or organ after the transplantation [17-19].

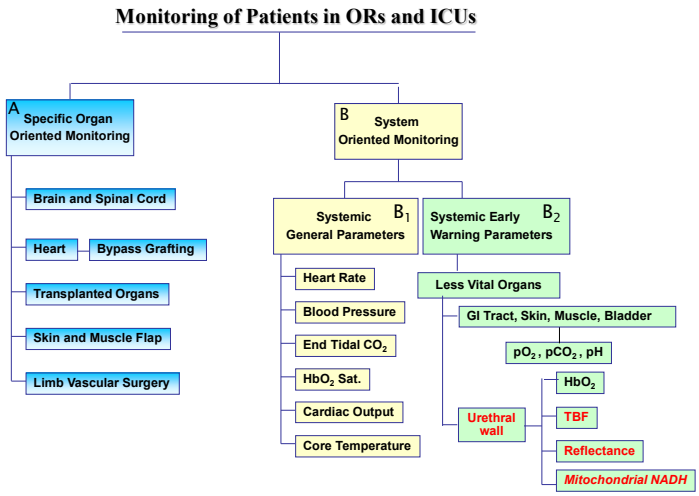

Figure 7: Patients monitoring takes place at two levels. A - Monitoring of the function of specific organs. B - Monitoring of systemic parameters. B1 – Systemic general parameters which are monitored today and B2 - systemic early warning parameters which could be monitored by the clinical devices developed.

The second approach in patient monitoring is shown in Figure 7B. This approach is divided into 2 subgroups labeled as B1 and B2. The parameters shown in B1 are measured routinely from the cardiovascular and respiratory systems. They provide information on systemic events, such as changes in respiratory gas exchange in the respiratory system or cardiac output affecting the perfusion of various organs in the body. Those parameters are used today in all ORs and ICUs as well as emergency departments. The second group of parameters, shown in part B2, is measured at the tissue level and the accumulated results represent the oxygen balance of the entire body. In this group of parameters, the monitored organs are defined as "less vital organ" as compared to the brain and heart that are "the most vital organs." One possibility is to measure the pO_2, pCO_2 or pH in various less vital organs and the information may be used as an early warning signal for a negative oxygen balance [20-22]. The 2nd approach is to monitor 4 parameters, including mitochondrial function in the urethral wall. The physiological mechanism behind the monitoring approach shown in part B2 of Figure 7 is illustrated in Figure 8. A clear example demonstrating the specific organ monitoring is shown in Figure 11 and 20.

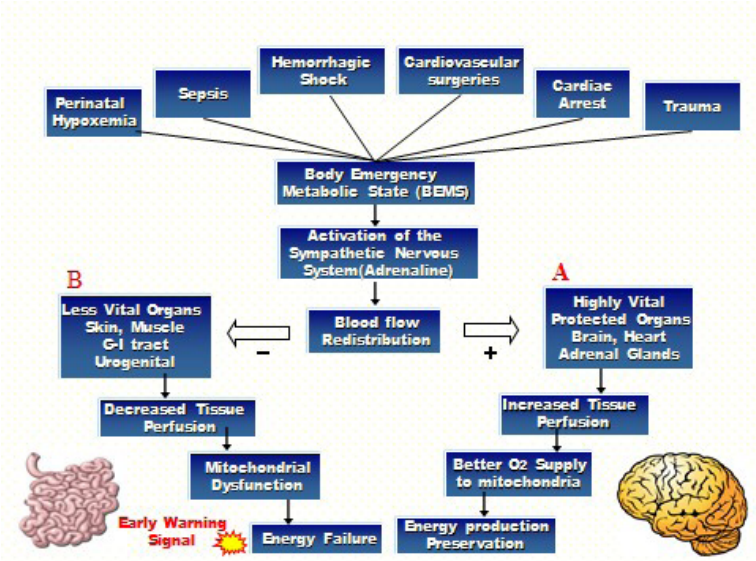

Figure 8: Schematic presentation of various pathological states developed under various clinical situations, which lead to the development of body emergency metabolic state (BEMS). As a result, blood flow redistribution will lead to an increase in blood flow to the most vital organs (A) and a decrease in blood flow to the less vital organs (B).

The pattern of pathophysiological cascade of events that may occur in many emergency clinical situations in adult patients and may lead to morbidity and mortality is shown in Figure 8. As shown, various pathological states may lead to metabolic disturbances and may result in cellular energy derangement [23-26]. The six pathological states, shown in the upper part of Figure 8, are the most common events that may develop in clinical practice. They may develop due to a specific salient event, such as a major operation or during a slow process of body deterioration, e.g. in sepsis or shock. The definitions of each of those 6 states are not so well established and some overlapping may exist. Under all those situations, the metabolic state of the body will be deteriorated and energy failure will develop. The situations shown in Figure 8 could develop in patients hospitalized in various operating rooms or intensive care units, as well as in emergency rooms. These include the respiratory, neurosurgical, cardiac and neonatal ICU. Also, all patients undergoing severe operations, such as cardiac bypass, neurosurgical or organ transplantation, may develop the Body Emergency Metabolic State - BEMS. Other patients that may develop BEMS are newborns during delivery or elderly patients treated in the internal medicine departments. As a central protection mechanism, blood flow redistribution will occur and the three protected organs (A - brain, heart and adrenal gland) will receive more blood and O_2, while the peripheral organs or areas (B - skin, G-I tract, Urogenital and muscles), as well as others less vital visceral organs, will undergo vasoconstriction and a decrease in blood flow and O_2 supply. Monitoring the cellular function is the most significant indicator of the metabolic state of patients in critical care medicine [27,28]. The energy balance in the most vital organs will remain positive due to higher blood flow, while the less vital organs will be hypo-perfused and a negative energy balance will develop. As presented in Figure 8, the blood flow redistribution mechanism will affect the energy production by the mitochondria in the most vital and less vital organs in the body. This change in mitochondrial function will affect the production of ATP.

Testing the "Blood Flow Redistribution" Hypothesis in Animal Models

In order to test the hypothesis termed "blood flow redistribution" under body emergency metabolic states, we developed an animal model mimicking the possible clinical situations.

The multi-site multi-parametric monitoring system (MSMP) monitors both NADH redox state using the Fluorometry technique and Tissue Blood Flow (TBF) using the Laser Doppler Flowmeter (LDF) simultaneously and from the same location on each organ (Figure 4,5 and 6) [29-31].

Methodology

In order to monitor NADH fluorescence, it is possible to use one of the two available principles. At the early stage, it was necessary to measure and identify the fluorescence spectrum of NADH. Fluorescence spectra were compared in different *in vitro* and *in vivo* preparations. In parallel, the second approach was adopted, namely measuring the total fluorescence signal accumulated and integrated into a single intensity value using appropriate filters. This approach was necessary in order to measure NADH fluorescence continuously. The fluorescence spectra of NADH measured in various *in vitro* and *in vivo* models by different investigators were summarized in 2007 [32]. In this review we will discuss the use of the real time monitoring approach and technology.

Principles of NADH Monitoring Technology

The origin of the fluorescence signal was proven to come mainly from the mitochondria. Also the comparisons between NADH fluorescence intensity and biochemical analysis of Pyridine Nucleotides were described in detail recently [32].

Since the early 1950s, different groups have developed a number of fluorometers adapted to their specific experimental protocols. As of today, most of the groups using NADH fluorometers construct the devices in house, since no suitable commercial products were available until recently.
The basic features of NADH fluorometers consist of the following:
1. A light source (including appropriate filters).
2. An optical path to the preparation and back to the detection unit.
3. Detection and signal processing units.
4. Signal recording and storage units.

DC NADH Fluorometer/Reflectometer

In our earlier reviews, published in 1984 and 2007, we extensively specified the light-guide-based fluorometry used in our studies [13,32]. The review article on *in vivo* NADH fluorescence monitoring, published in 1992 by Ince *et al.*, included many other technical aspects of the methodology [33]. In order to enable the monitoring of NADH fluorescence in unanesthetized animals or other *in vivo* preparations, a flexible means was needed to connect the fluorometer with the tested tissue in the organ, for example the brain. This was achieved in 1972, when UV transmitting quartz fibers became available (Schott, Jena Glass, Germany). Our group developed and used the model shown in Figure 9A in the late 1970's. This model is still being used in our laboratory to monitor the brain, heart, liver, kidney and other organs [32].

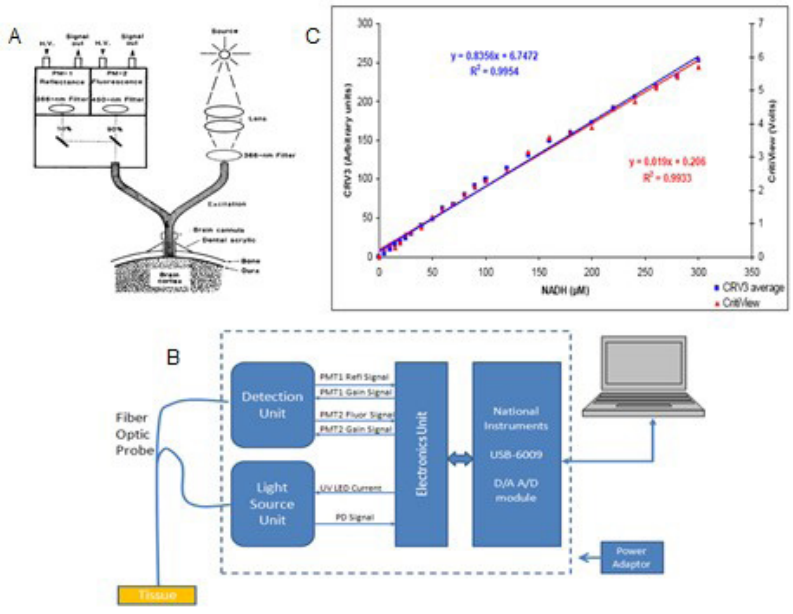

Figure 9: The structure of two types of fiber optic based fluorometers. A - Standard research DC fluorometer/reflectometer in the upper part of A. Fiber optic probe is connected to the brain of a small animal. In part B, a commercial device (made by Prizmatix Ltd, Israel) is presented. C - Fluorescence readings (2 sets) of two fluorometers plotted against NADH concentration after subtracting the reading of the blank solution. A linear regression was calculated, and the equation and R2 are presented for the 2 sets of control solutions.

Device calibration studies reveal that the range of 0 to about 300 μM NADH in solution (*in vitro*) provides a linear correlation with the fluorescence levels. Two sets of solutions with known concentrations of NADH in Double Distilled Water (DDW) were prepared and measured by the developed monitoring device. The results of the readings were plotted against NADH concentrations and are presented in Figure 9C. A linear regression was calculated for each line and the linear equation and R^2 are presented in the graph.

The Factors affecting NADH fluorescence and reflectance signals were described in details in 2007 [32]. The excitation and emission spectra of NADH are affected by the redox state of this fluorochrome and by other factors, leading to artifacts in the fluorescence measurements. In this section, various NADH unrelated factors, affecting the measured signal, will be discussed. Since most fluorometers involve the measurement of the total backscattered light at the excitation wavelength (i.e. 366 nm), the discussion will concern changes in NADH fluorescence as well as in tissue reflectance.

The following factors may affect the two measured signals, 366nm reflectance (R) and 450 nm fluorescence (F):
1. Tissue movement due to mechanical or intracranial pressure changes.
2. Extracellular space events, such as volume changes or ion shifts between intra- and extra-cellular spaces.
3. Vascular and intravascular events, for example, oxy-deoxy Hb changes, and blood volume changes due to autoregulatory vasoconstriction under pathological conditions.
4. Intracellular space factors, such as O_2 level, ATP turnover rate, substrate availability, and mitochondrial redox state.

As of today, a new approach is still lacking to compensate for non-NADH factors affecting the NADH fluorescence signal. We have found that subtracting the reflectance from the fluorescence or dividing the two parameters provides similar net NADH changes. Bradley & Thorniley published a review article dealing with the various correction techniques for tissue fluorescence. They summarized their review by the following conclusion: "even though research has been conducted into correction techniques for over thirty years, the development of a successful and practical correction technique remains a considerable challenge [34]."

A new fluorometer/reflectometer device (MitoViewer) was developed in 2007 by an Israeli company- Prizmatix Ltd., as seen in Figure 9B. The MitoViewer system comprises the following main subunits:
1. Light Source Unit – provides UV light at 365 nm for NADH fluorescence excitation and tissue reflection measurements. Also included is a reference photodiode that enables correction of signals in cases of intensity changes of the LED during measurement. Fiber Optic Probe – transmits the UV light from the Light Source Unit to the measured tissue site and transmits the collected light (the reflection (Refl) and the fluorescence (Fluor) from the tissue, to the Detection Unit.
2. Detection Unit – provides detection to transform the Reflectance and Fluorescence light into electrical signals which are transmitted to the electronics board for amplification.
Electronics Unit – provides amplification for the Reflectance and Fluorescence signals as well as control of the detector gain and driver for the UV LED. The amplified signals are transmitted to Analog to Digital convertor module.USB-6009 module – provides Analog to Digital (A/D) conversion for the two signals and Digital to Analog (D/A) conversion for control signals sent from a PC to control the function of the MitoViewer.
3. PC – Personal Computer enables control of the MitoViewer operation through the MitoViewer software.
4. Power Adaptor – provides the DC voltage for operation of the MitoViewer.
The fiber optic probe of the MitoViewer was attached to the surface of the brain via an appropriate holder cemented to the skull with dental acrylic cement.

Animal Preparation for NADH Monitoring

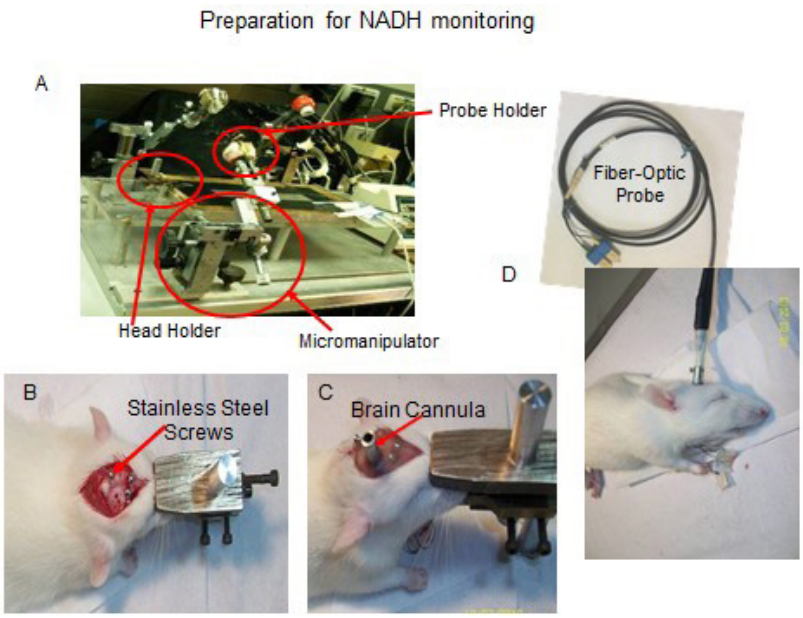

Figure 10: A - The system used to prepare and monitor up to 4 organs simultaneously. The same system enables researchers to perform a craniotomy while the animal is connected to a special head holder. B-D - Stages in the preparation of the rat brain for NADH monitoring. **B** - Location of screws enabling the fixation of the light guide holder to the skull by dental acrylic cement. **C** - The view of the skull after the end of the operation. **D** - After the insertion of the fiber optic probe to its holder the animal is ready for the monitoring.

A special table and probe holding device was constructed in order to perform brain as well as other organs preparation for the monitoring period. The device for the operation procedure is shown in (Figure 10A). The brain is operated while the head is connected to a special head holder for the period of the operation (20-30 minutes) and then could be released, for the monitoring period, as shown in (Figure 10B and C). The other monitored organs i.e. muscle, kidney or liver, have to be held by a micromanipulator during the monitoring period. As mentioned before, the brain was the main organ monitored by other investigators as well as in our group. As an example, the entire protocol of the preparation of the rat and the exposure to various perturbations is given here in detail. Adult male Wistar rats (250–350g) were anesthetized by intraperitoneal (IP) injection of Equithesin solution (each mL contains: Chloral Hydrate 42.51 mg, Propylene Glycol 44.34%, Pentobarbital 9.72 mg, Magnesium Sulfate 21.25 mg, Alcohol 11.5% water) 0.3 ml/100g body weight. A midline incision is made in the skin, exposing the skull. Three holes were drilled in the skull and appropriate small screws were inserted to the skull (less than 1 mm in depth) as shown in figure 10B. An appropriate craniotomy (3-5 mm in diameter) was drilled in the right or left parietal bone for the fixation of a light guide holder in which the monitoring probe was inserted later on. The light guide holder and the 3 screws were then fixated to the skull using dental acrylic cement (Figure 10C). Ten minutes later the head of the animal was released from the head holder and the probe was inserted to a predetermined depth and fixed by a set screw (Figure 10D).

Monitoring of Patients in Neurosurgical OR

A new commercial device was developed in the early 2000s. In the new device - the Tissue Spectroscope (TiSpec), we monitored three parameters representing the microcirculation and the intracellular mitochondrial function [35]. The TiSpec provided information collected from the microcirculation (blood flow and volume) and the intracellular space (mitochondrial NADH) (Figure 11A). The TiSpec and the various probes developed for this device are presented in (Figure 11). This device was tested in animal models as well as in neurosurgical patients. Figure 10D shows a needle type probe used for monitoring the brain of experimental animals. In (Figure 11B), a specific holder and a fiber optic probe is shown connected to the neurosurgical patient in the OR by a micromanipulator. More details regarding the Tispec were published [36,37].

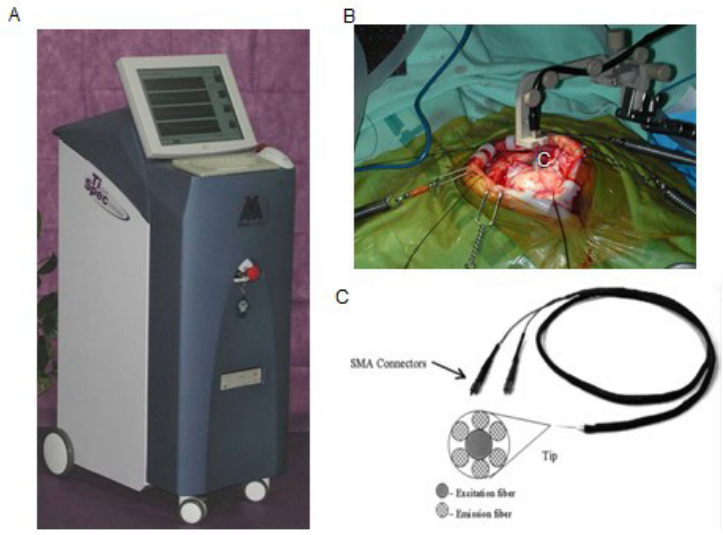

Figure 11: Monitoring of a neurosurgical patient in the operating room. **A** - The tissue spectroscope device. **B** - Location of the optical probe tip on the brain. **C** - A standard, pencil type, fiber optic probe.

Multisite/Multiparametric (MSMP) Monitoring System

In order to monitor more than one parameter and in more than one organ at the same time, we developed the MSMP monitoring system. Each of the 2 channels of this monitoring device contains a bundle of optical fibers for NADH redox state monitoring using the fluorometric technique, and another bundle of fibers for tissue blood flow (TBF) monitoring using Laser Doppler Flowmeter) Figure 12A and B). The diameter of the probe (including all fibers) is 3 mm. The principle of NADH monitoring from the surface of the tissue (1 mm depth) is that excitation light (366 nm) passes from the fluorometer to the tissue via a bundle of optical fibers made of quartz. The emitted light (450 nm fluorescence), along with the reflected light (366 nm reflectance), is transmitted to the fluorometer via another bundle of fibers [13]. The emitted light passes through appropriate filters in order to differentiate between 366 nm reflectance and NADH fluorescence (450 nm). In addition, a specific filter is used in order to prevent red light (laser Doppler flowmeter) from interfering with mitochondrial NADH monitoring. Changes in the reflected light are correlated to changes in tissue blood volume and therefore serve to correct for hemodynamic artifacts in NADH monitoring [32]. The corrected fluorescence (NADH) is obtained by subtracting the reflectance from the fluorescence signal at a 1:1 ratio. Tissue blood flow was monitored using a laser Doppler flowmeter, based on the Doppler shift reflecting the flow of red blood cells in the microcirculation in a depth of 1-2 mm [16,32,38]. All the signals monitored during the experiment were digitized and transmitted to a multi-channeled computerized data acquisition and recording system (Labview A/D software, National Instruments Inc).

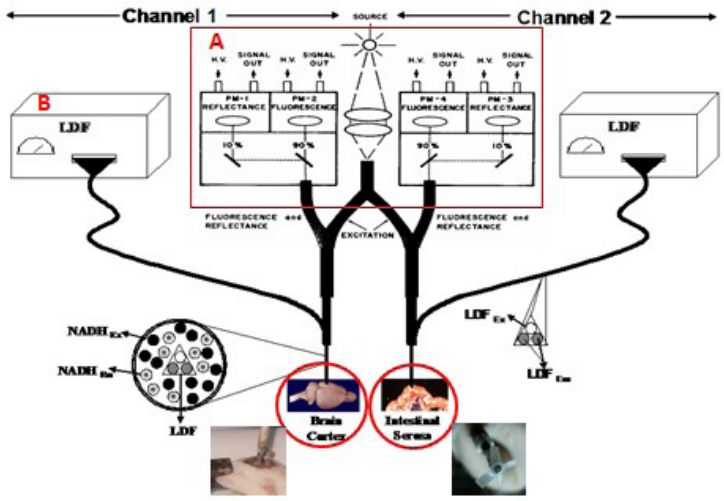

Figure 12: Schematic representation of the 2-sites monitoring system containing optical fibers for NADH monitoring (Ex – Excitation, Em – Emission, H.V. – High Voltage) and for tissue blood flow (Laser Doppler Flowmetry – LDF). In this study the brain and small intestine were monitored.

All experiments were performed in accordance with the Animal Care Committee of Bar-Ilan University Guidelines. Wister male rats (220–300g) were anesthetized by an IP injection of 0.3 ml/100 gr of Equithesin (each ml contains: pentobarbital 9.72 mg; chloral hydrate 42.51 mg; magnesium sulfate 21.25 mg; propylene glycol 44.34% w/v; alcohol 11.5 % and water). During the entire experiment, the rats were maintained anesthetized by an addition of 0.1ml Equithesin every half hour. In addition, a heating pad was placed under the rat to maintain body temperature at 37 °C and a rectal thermistor probe (Yellow Springs Instruments Co. Inc.) was inserted for body temperature measurements.

Preparation of the brain for monitoring was described in section 5.3. For the exposure of the small intestine, an abdominal mid-line incision below the rib cage was created. Then, a small part of the ileum was exposed and placed above a special plastic holder. Afterwards, the probe was placed on the ileum's serosa using a micromanipulator, with assistance of a small piece of parafilm and cyanoacrylate adhesive. Finally, a slice of parafilm was placed around the probe and over the incision to prevent dehydration and a black cloth was placed above to avoid room light from entering the monitored site and causing artifacts.

Development of the Small Intestine Monitoring Model

During the developing of the 2 organ monitoring model, the question arose where to place the probe for intestinal monitoring. To resolve it, we tested 2 experimental models, in which one probe was placed on the serosa and the other on the mucosa (Figure 13C). The first experimental model involved short anoxia, i.e. inhalation of 100% N_2 until the rat stopped breathing. The second model involved IV injection of 6μg/kg epinephrine. In both models, the responses of the serosa and mucosa were compared.

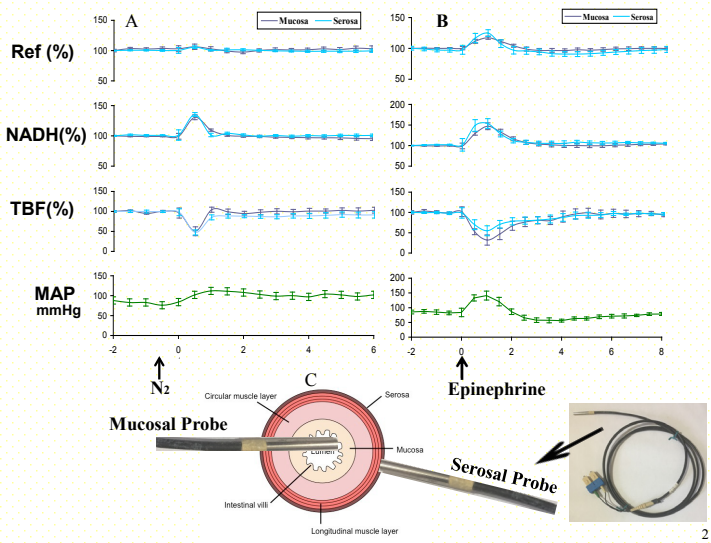

Figure 13: A - The responses of blood pressure, mucosa (dark blue) and serosa (light blue) during short anoxia (n=8, mean ± S.E.). Ref - reflectance, NADH - mitochondrial NADH redox state, TBF - tissue blood flow, MAP - mean arterial pressure. **B** - The responses of the MAP, mucosa (dark blue) and serosa (light blue) during injection of epinephrine (n=8, mean ± S.E.). **C** - The 2 tips of the fiber optic probes that are connected to the mucosal and serosal sides of the small intestine wall.

Figure 13A presents the responses of the serosa and mucosa to short anoxia. MAP increased, and both layers of the intestine, the serosa and mucosa, responded by a decrease in TBF and increase of NADH. No significant differences were observed between the two layers. Figure 13B represents the responses of the serosa and mucosa to I.V. injection of epinephrine. As it is seen, both intestinal layers responded similarly to epinephrine. MAP increased, TBF decreased, and both the reflectance and NADH increased. Furthermore, no significant differences were observed between the two layers. According to these results, showing no significant differences between the serosa and mucosa, we decided to place the intestinal probe on the serosa, since it is less invasive and easier to manipulate.

Monitoring of Patients in Critical Care Medicine - The CritiView

During the last 20 years we were able to develop three generations of medical device that were used in various patients according the scheme shown in (Figure 7 and 8). The last model that was developed - the "CritiView" - was tested in patients and was also cleared by the FDA. The aim was to develop a small device that will fit the minimal free space available in ORs and ICUs as seen in (Figure 14). The CritiView device performs real-time continuous spectroscopic measurements as presented in (Figure 14,15 and 16). It transmits light at specific wavelengths through the tissue and measures fluorescence, Doppler shift, and intensity of the light reflected back from the tissue. The four parameters are calculated as follows:

a. Mitochondrial NADH fluorescence emitted at 420 nm to 480 nm.

b. Total backscattered light (375 nm) reflected from the tissue (R). This parameter allows for correction of the NADH fluorescence measurement due to changes in tissue blood volume.

c. Doppler shifted laser light (785 nm) reflected from moving blood cells, indicating tissue microcirculatory blood flow (TBF).

d. HbO_2 - Oxygen saturation of hemoglobin (470 nm, 525 nm). This parameter was not measured in all monitored patients.

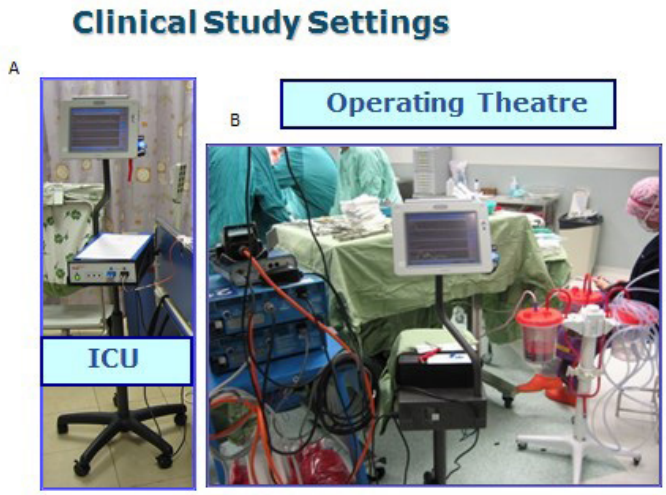

Figure 14: The CritiView device used in the ICU (A) and in the operating room (B).

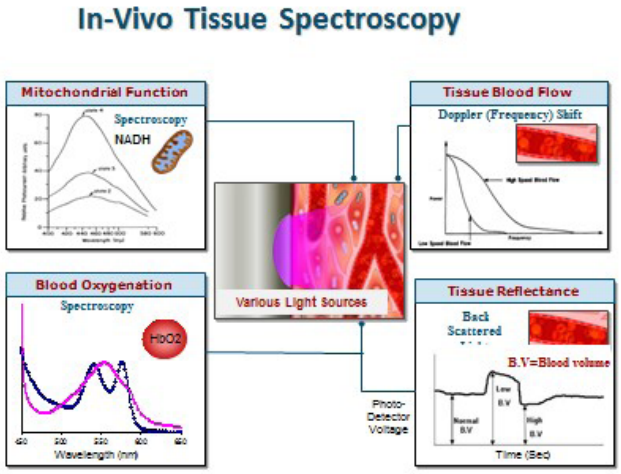

Figure 15: The principles of tissue spectroscopy in order to evaluate tissue viability by the CritiView (A). Three of the parameters are monitored from the intravascular compartment while the NADH parameter represents the function of the intramitochondrial space.

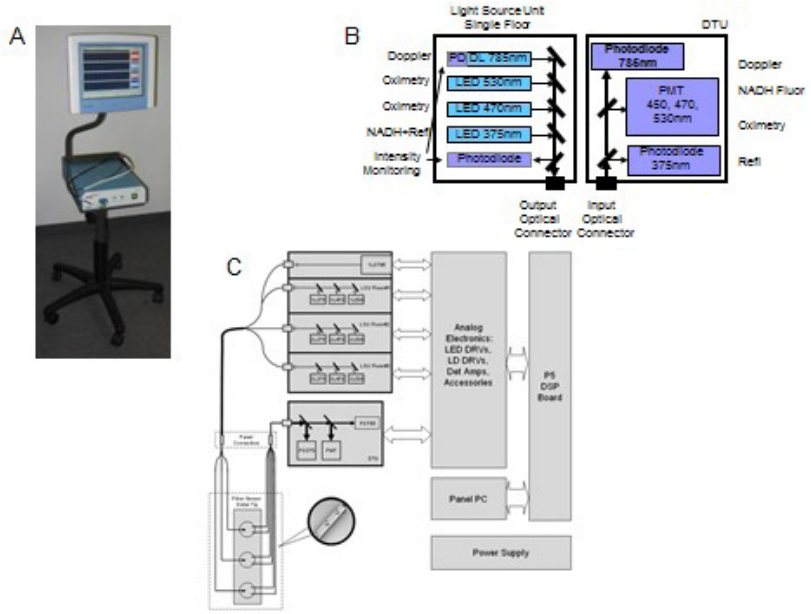

Figure 16: A - The standalone compact CritiView device is shown in part A. **B** - Detailed schematic description of one of the floors of the CritiView containing the light source unit (LSU) and the detection unit (DTU) are presented. **C** - The basic features of the CritiView developed for experimental and clinical use.

The light source unit comprises a 785 nm CW laser diode which serves for laser Doppler measurement, a UV LED (375 nm) for NADH fluorescence excitation and for total back scatter (or reflection) measurement, a blue LED (470nm) and a green LED (530 nm) for HbO_2 (Figure 16B). In order to enable a very high measurement dynamic range of fluorescence and reflection parameters, the light source unit is designed to enable a very wide range of the excitation intensities. To enable this wide excitation range and linearity, the system is designed according to a three floors concept. Each floor comprises three LEDs one UV LED with emission peak at 375 nm, one blue LED with emission peak at 470 nm and one green LED with emission peak at 530 nm. The different wavelengths from all LEDs of the same floor are assembled together and coupled into a single fiber by a set of dichroic mirrors and appropriate collimation and focusing lenses. The current of each one of the discrete LEDs is set by the appropriate electronics drivers directly controlled by a D/A of the DSP processor. The difference between the floors is the output intensity. There is a High, Medium and Low intensity floors. The different excitation intensities are achieved by utilizing various pinholes while maintaining all other electro optical properties as the same for all three floors. The light from all the three floors and a laser diode are combined into a single mixer fiber, therefore enabling precise setting of the excitation intensity within a very wide excitation range. The near IR laser diode at 785 nm, for laser Doppler measurements, operates in Continuous Wave (CW) operation mode. The UV LEDs, blue LEDs and green LEDs operate in chopping mode. This enables the use of synchronous detection techniques in order to detect the NADH fluorescence and total backscatter light.

The Detection Unit (DTU) All six collection fibers of the fiber optic probe are assembled into a single male SC optical connector (Figure 16C). The light from the probe passes though the panel connector into a single thick optical fiber that delivers the light to the DTU. At the DTU entrance the collimation lens collimates the fiber output light. The collimated light is split according to the different wavelengths into the respective photo detectors by means of dichroic beam splitters. The first dichroic beam splitter reflects the total backscatter signal at 375 nm towards the photodiode detector. The higher wavelengths pass through the first beam splitter towards the second dichroic beam splitter. The second dichroic beam splitter reflects the NADH fluorescence signal at 450 nm and total backscatter signals at 470 nm and 530 nm towards the photomultiplier detector. Due to the chopping operation of the LED's the photomultiplier detector detects each one of the above-mentioned signals at a different time, i.e., time sharing operation detection mode. The second dichroic filter enables the laser Doppler signal at 785 nm to pass through it towards the photodiode detector. All acquired signals are digitized into the DSP processor by high resolution 16 bit A/D.

The DSP processor is responsible for whole system control, initial data processing and calculation of the Doppler parameter. The DSP is built around Tern Inc. 586-Engine-P controller board with AMD SC520 CPU. After initial data processing, the calculated values are transmitted to the panel computer for final data processing display through RS-232 serial interface. The CritiView device utilizes medical grade main power supply for all electronic circuits including the panel computer.

Using the CritiView in Patients: In order to monitor less vital organs in patients, we developed a "smart" Foley catheter seen in (Figure 7,8 and 17A). The Foley catheter optical probe for measuring the urethral wall vitality is presented in (Figure 17B). It is based upon a standard 3 lumen Foley catheter (the Foley catheter is an inflatable balloon retention type catheter inserted through the urethra, and used to drain the bladder). This probe construction enables the measurement of tissue metabolism at the urethral wall, while draining the bladder. The Foley catheter optical probe is designed to perform optical measurements from three adjacent points on the tissue 3.5 mm apart. Each measurement point is comprised of one excitation fiber and two adjacent collection fibers. The 3 excitation fibers from the LSU are connected to the excitation connector on the CRV panel. All 6 collection fibers from the three measurement points are connected to the single collection connector on the CritiView front panel. Figure 17C shows the finished probe inside the Foley catheter. The location of the monitoring points in a female patient was adapted to the shorter urethra. Figure 17D and E present the positioning of the 3-way Foley catheter (containing the fiber optic sensors) inside the urethra and the bladder of a male patient.

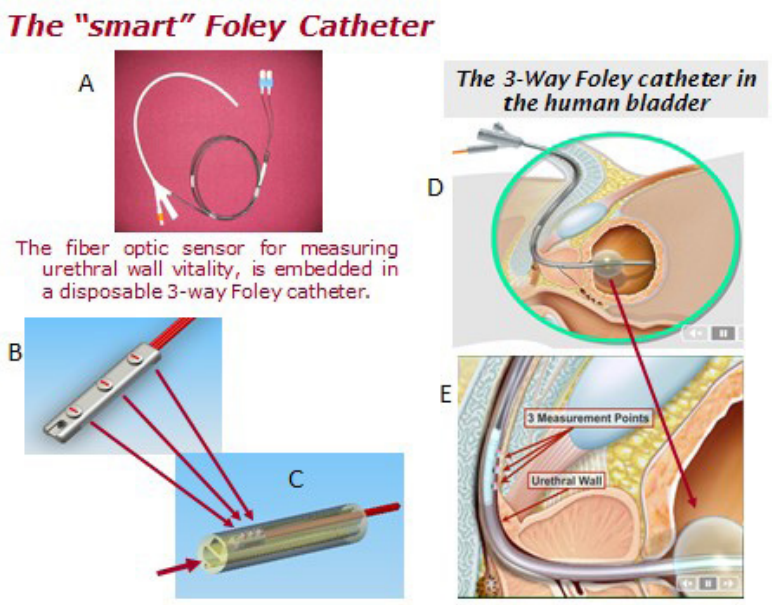

Figure 17: A - The Foley catheter used for patients' monitoring. **B** - Tip of fiber optic probe showing the monitoring points. **C** - The cross section of the catheter. D and **E** - The location of the 3-way Foley catheter and the monitoring sites in the urethral wall of a male patient.

Results

Effects of Oxygen Supply on Brain NADH Redox State

The effects of changes in oxygen supply are presented in (Figures 18 and 19). We define anoxia as a complete deprivation of O_2 caused by breathing 100% N_2. Hypoxia implies that the deprivation of O_2 from the breathing mixture is partial and ranges between 21% (normal air) and 0% (anoxia). Ischemia is defined as a decrease in O_2 supply due to a decrease in blood flow to the brain. The degree of ischemia can vary from a complete absence of flow (complete ischemia) to various levels of blood flow (partial ischemia). Although oxygen deficiency is the main event in each of the three experimental conditions (anoxia, hypoxia and ischemia), other physiological factors may differ. For example, microcirculatory blood flow is decreased under ischemia, but increases under brain hypoxia. Thus, changes in the tissue due to other blood flow related factors are not identical. According to the definition of Chance & Williams a shift toward State 5 involves

an increase in NADH proportional to a decrease in O_2 supply [14]. As shown in Figure 18A when the brain was exposed to 100% N_2, the fluorescence (F, CF) showed a clear increase-decrease cycle depending on the availability of O_2 [13,41]. In auto-regulated blood-perfused brain, it is expected that the lack of O_2 will trigger compensation mechanisms that may lead to an increase in the blood flow and volume, or a decrease in the R signal. The results are shown in Figure 18A, and indeed, R exhibited a large decrease due to the increase in blood volume (vasodilatation of brain vessels). The electrical activity of the brain disappeared under anoxia due to the lack of energy. The effect of severe ischemia presented in Figure 18B is very similar in the response of the corrected fluorescence signals - CF to that seen under anoxia.

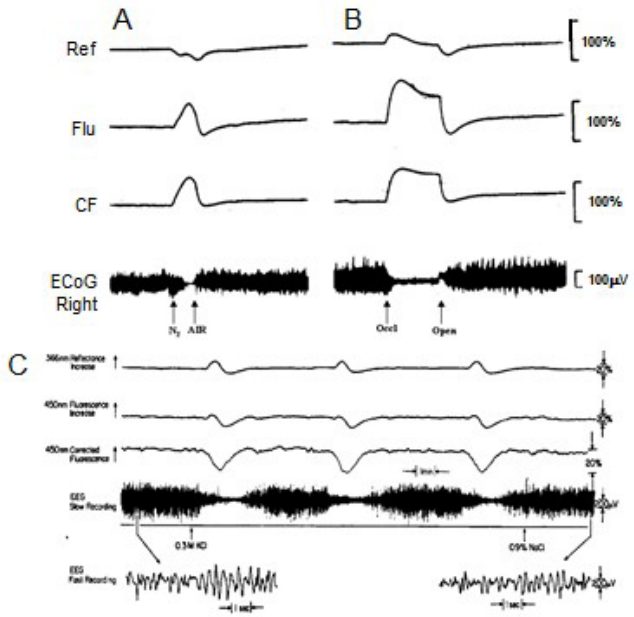

Figure 18: A - Responses to complete deprivation of oxygen (anoxia) on brain NADH redox state. **B** - The effects of severe ischemia on brain NADH redox state. **C** - Repetitive response of the brain to spreading depression evoked by application of 0.3 M KCI on the dura. The third trace is on an expanded amplitude scale. The arrow direction shows an increase in the optical signals. Time proceeds from left to right. Three cycles of oxidation of NADH were developed.

Figure 19A shows the effects of hypoxia (6% O_2) and hyperoxia (100% O_2) on NADH redox state monitored by the MitoViewer described in section 5.2. The NADH was elevated in hypoxia and decreased (oxidized) during hyperoxia.

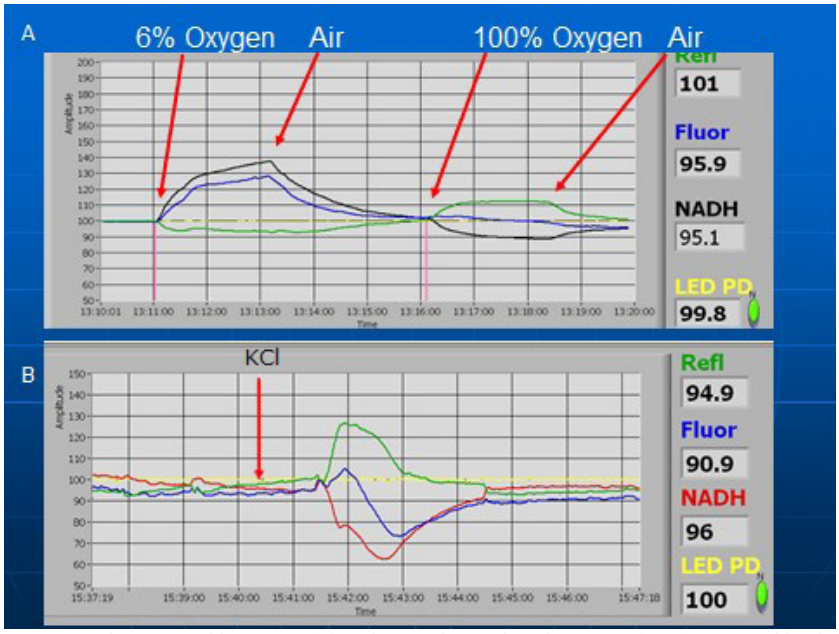

Figure 19: Responses to hypoxia and hyperoxia (A) and cortical spreading depression (CSD) measured by the commercial device - MitoViewer (see text for details).

Responses of NADH to Brain Activation

The activation of the mitochondria by increased ADP is coupled with oxidation of NADH (decreased NADH levels), and is known as the State 4 – State 3 transition in isolated mitochondria. We will describe the effects of tissue activation on NADH fluorescence under normoxic conditions. Since the discovery of brain Cortical Spreading Depression (CSD) by Leao in 1944, it has become clear that the wave of depolarization passing through the tissue, increases energy consumption [42,43]. The effects of CSD on brain mitochondrial NADH was described in 1973 and a clear oxidation wave was recorded [41]. This stimulation of the respiratory chain will increase oxygen consumption and, consequently, blood flow will be increased to compensate for the extra oxygen needed [44]. Extra oxygen supply or compensation can be achieved by either an increase of CBF, enhanced O_2 extraction, or both. In a well-controlled study, we showed that concomitantly to NADH oxidation and extracellular K+ changes, CBF doubled while oxygen extraction ratio remained the same [44]. Typical responses to CSD monitored in the brain of an awaken rat are shown in Figure 18C where the correlation between the depression of electrical activity (ECoG) and the oxidation (decrease) of NADH, in 3 repetitive cycles is clear. The relationships between changes in various parameters developed during CSD were reported in many publications (see Review) [32]. The initial events in CSD are changes in electrical (ECoG and DC potential) and ionic homeostasis (elevated extracellular potassium). The response to those changes is the activation of ion pumps that increased energy consumption. The NADH is more oxidized and blood flow to the brain is elevated. The same responses to CSD were recorded when NADH was monitored by the MitoViewer as seen in (Figure 19B).

Responses of Patients in the Neurosurgical OR

In order to demonstrate the potential use of our technology in clinical neurosurgery we present the following results. When Papaverine was locally injected, CBF increased and a small oxidation of NADH was observed (Figure 20A). In another patient, an aneurysm in one of the small brain arteries was treated in the OR. The response to placing a clip on the artery shown in Figure 20B was similar to ischemic event, namely a decrease in CBF and a clear increase in NADH.

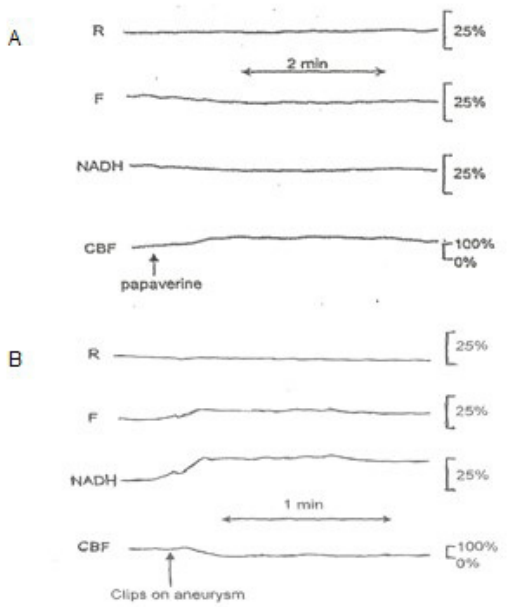

Figure 20: A - Responses of the human brain during surgery. The effect of papaverine on NADH and CBF (A). **B** - Effect of local ischemia induced by a surgical clip placed on a brain artery with aneurysm.

Physiological Responses of the Brain and Intestine to Various Perturbations

Testing the effects of partial oxygen deficit - hypoxia on the brain and small intestinal metabolism showed the following results (Figure 21A). MAP decreased by 34±4 mmHg ($p<0.001$) immediately after the rats started breathing the low oxygen mixture. This change was followed by a decrease in TBF in the intestine to the level of 57±15% ($p<0.05$), and a tendency of CBF increase to the level of 130±13%.

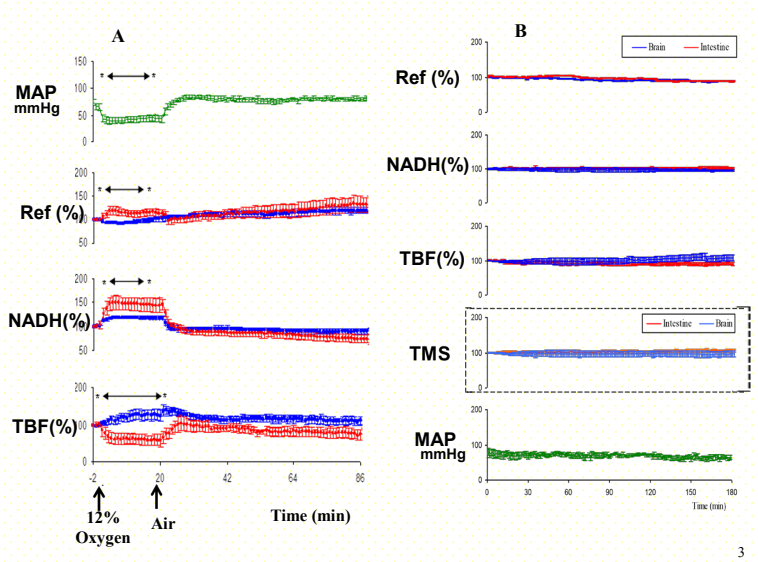

Figure 21: A - The responses of the brain (blue) and small intestine (red) to hypoxia (12% oxygen in air). Abbreviations are as above in Figure 13. Two organs were monitored simultaneously. Arrows show the period of time in which differences between both organs were significant for each minute. (N=9). (*) $p<0.05$. B - monitoring of normotensive rats: the brain (blue) and the small intestine (red) in the group (n=4). Ref - reflectance, NADH - mitochondrial NADH redox state, TBF-tissue blood flow, MAP - mean arterial pressure. Index - calculated Tissue Metabolic Score.

Simultaneously, the reflectance in the intestine increased (10±8%, $p<0.05$), while in the brain it decreased (92±2%, $p<0.01$). The changes in blood supply to the organs produced corresponding changes in the levels of mitochondrial NADH. In the intestine, NADH increased to the level of 150±14% ($p<0.01$) and remained at this level through the entire hypoxic period, while in the brain NADH reached the level of 119±2% ($p<0.01$). When the rats started breathing air, all parameters returned to the basal level within 2 minutes in the intestine, whereas in the brain hyperemia was observed for 11 minutes followed by a full recovery.

Monitoring of a vital and less vital organ in normotensive rats is presented in Figure 21B (control monitoring of the brain and the intestine) including 4 rats. This group was monitored for 180 minutes, with no perturbations induced during the entire monitoring period. For the entire trial, there were no significant changes in any of the parameters, or only very minute ones in comparison to the base line and between the two organs.

Data Interpretation using the MSMP Monitoring System: As of today, there is a discrepancy between the large amount of data collected by various techniques and the ability to integrate it into a practical objective tool to be used in experimental and clinical practice. Our effort to apply our developed multiparametric system to future clinical daily use required the development of a new indexing technique to help data interpretation. After the accumulation of vast amounts of experimental results, we decided to develop a new tool named Tissue Metabolic Score (TMS). We have developed TMS that could be used in evaluating the vitality of the monitored tissues.

Since the main purpose of the TMS is to give an indication for the metabolic state of a tissue or an organ, and since oxygen is a major factor in tissue viability, it is obvious that this index should include the combination between tissue oxygen supply and demand. The mitochondrion is the cell energy factory, and mitochondrial NADH is the most sensitive indicator for oxygen balance [45-47]. Thus, we believe that the NADH should get the highest importance in a formula providing the TMS. Figure 21B (4^{th} trace) shows the calculated TMS recorded in a control rat monitored for 3 hours. The stability of the TMS was very high and no difference between the brain and small intestine was noted.

Testing the concept of "Blood Flow Redistribution": In order to test the hypothesis of the "blood flow redistribution," we compared the responses of the brain and small intestine to the level of anesthesia used in a rat model subjected to epinephrine injection. We chose the 6 μg/100 gr B.W. dose since this was the dose which yielded the maximum response of MAP and TBF as seen in (Figure 22). A group of 9 rats was injected with pentobarbitone to induce deep anesthesia. The systemic changes during the first 2 minutes post epi-

nephrine injection were similar under both levels of anesthesia. However, in the last 2 minutes MAP in the mild anesthesia group was significantly higher (75±4 mmHg, p<0.05) than the MAP in the deep anesthetized group (58±4 mmHg, p<0.05) due to an increase of this parameter at the beginning of the second minute post epinephrine injection. The hemodynamic and metabolic changes in the deeply anesthetized rats' cerebral hyperemia (228±21% vs. 172±15%; p<0.05) and NADH oxidation (80±1%; p<0.05) were larger than in the mild anesthetized rats (86±1%, p<0.05) (Figure 22A). Nevertheless, the pattern of response to epinephrine injection was similar under these two levels of anesthesia. In contrast, in the intestine there were no differences between these two levels of anesthesia (Figure 22B). Intestinal blood flow in the mildly and deeply anesthetized rats decreased to the level of 42±14% and 45±15% respectively (p<0.01). Consequently, NADH increased to the level of 143±8% and 137±8% respectively (p<0.01). Intestinal reflectance increased in both groups to the level of approximately 120% (p<0.01).

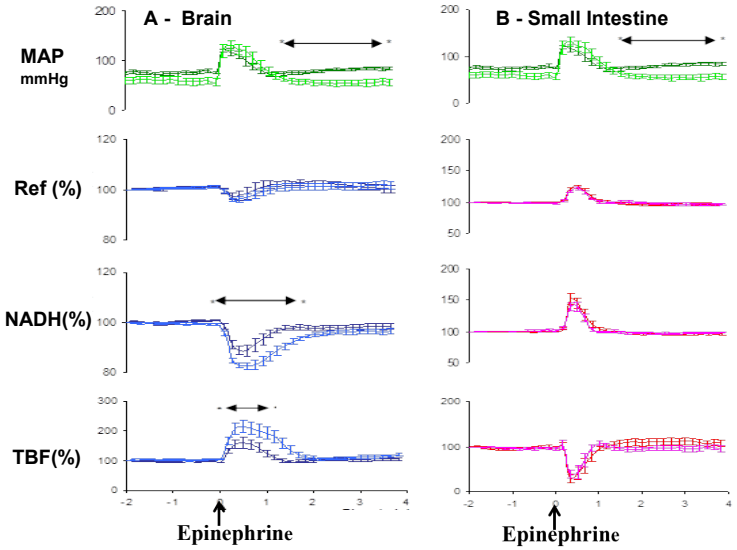

Figure 22: A - The responses of the brain to Epinephrine (6 µg/100g IV) under mild anesthesia (blue) and deep anesthesia (light blue). For MAP mild anesthesia (green) and deep anesthesia (light green). Arrows show the period of time in which significant differences between the two responses were detected. Abbreviations are as in Figure 13. (N=9). (*) p<0.05. **B** - The responses of the small intestine to Epinephrine (6 µg/100g) under mild anesthesia (red) and deep anesthesia (pink). For MAP mild anesthesia (green) and deep anesthesia (light green). Arrows show the period of time in which significant differences between the two responses were detected. (N=9). (*) p<0.05.

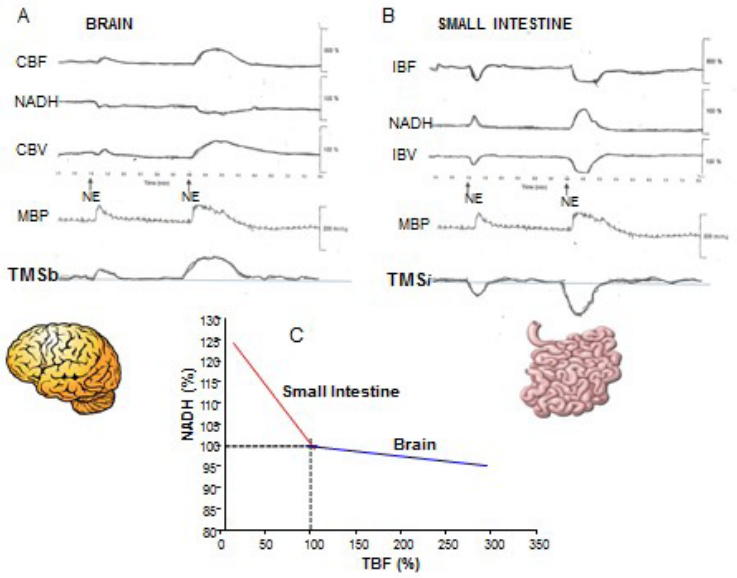

Figure 23: The responses of the Brain (A) and small intestine (B) to two levels of norepinephrine injected to the anesthetized rat. C - The correlation between the tissue blood flow (TBF) and NADH in the organs monitored. CBF and CBV - Cerebral blood flow and volume measured by a laser Doppler flowmeter, MBP - Mean blood pressure, IBF and IBV - Intestinal blood flow and volume, TMSb and TMSi - Tissue Metabolic Score calculated for the brain and small intestine.

The utility of the calculated tissue metabolic score (TMS) is presented in (Figure 23). In the rat used in the study, the brain and small intestine were monitored under the injection of two levels of norepinephrine (NE). The effect of the NE led to a clear increase in blood pressure depending of the dose injected. The responses of the 3 parameters measured in the two organs were in the opposite directions. In the brain, the clear increase in CBF and CBV was correlated to the oxidation of NADH redox state (Figure 23A). In the small intestine the NE led to opposite responses compared to the brain (Figure 23B). The tissue metabolic score that was calculated, as seen in the lower records (TMS), shows clearly that the less vital organ is clearly exposed to ischemia, while the brain is preserved and well oxygenated under the NE injection. In part C of Figure 23, the correlation between tissue blood flow and NADH after injection of NE is presented.

The Effect of Hemorrhagic Shock: The same approach developed for the calculation of the TMS was tested in one of our experimental protocols. The technology and animal preparation details were published elsewhere [48]. In the specific protocol shown in Figure 24, the rat was exposed to 60 minutes of controlled hypotension. Under controlled 40 mmHg hypotension maintained for 60 minutes, only 7 rats out of 13 survived. Figure 24 shows the averaged responses of those rats. The hypotension was induced by bleeding out 45±4% of the rats' total blood volume. During bleeding, MAP sharply decreased by 51±0.5 mmHg ($p<0.001$). Both TBF's decreased rapidly and stabilized at low levels. However, while IBF significantly decreased by 61±6% ($p<0.001$) CBF significantly decreased only by 45±5.5% ($p<0.01$). Intestinal reflectance showed a trend of increase, while the cerebral reflectance increased by 5±2% ($p<0.05$) and decreased back to its basal level. In comparison to the intestinal NADH, which slowly increased up to 228±24% ($p<0.01$), cerebral NADH increased only to a level of 142±5% ($p<0.01$). The maximum levels of NADH in both organs were monitored at the end of the hemorrhagic period and were also associated with the maximum changes in TBF.

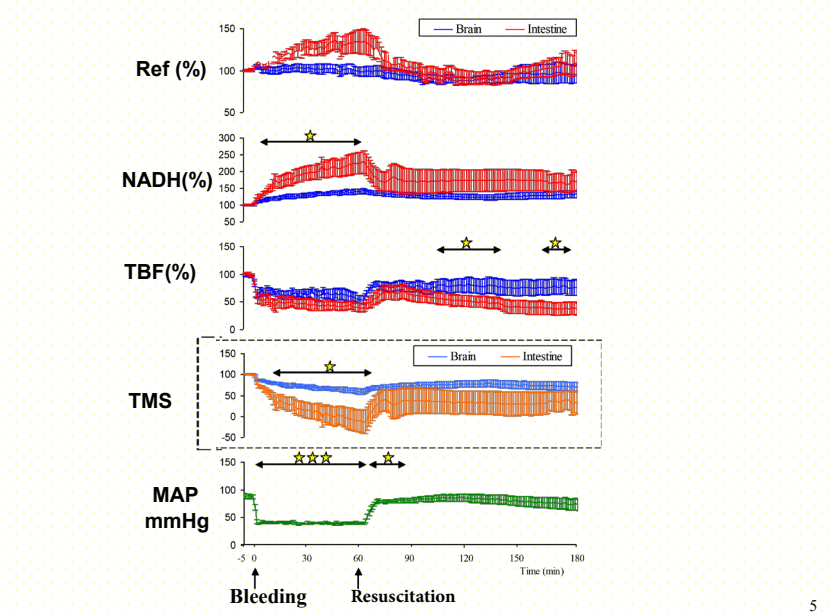

Figure 24: The responses of the brain (blue), small intestine (red) and mean arterial pressure (MAP) to controlled hypotension for 60 minutes in a group (n=7, mean ± S.E.). The arrows represent the period in which significant differences were found between the two organs and the asterisks represent significance levels: *p<0.05, **p<0.01 and ***p<0.001. Asterisks in Ref, NADH and TBF mark significance between brain and intestine; asterisks in MAP mark significance compared to baseline. Ref - reflectance, NADH - mitochondrial NADH redox state, TBF - tissue blood flow, MAP - mean arterial pressure. Index - calculated Tissue Metabolic Score (TMS).

Following resuscitation, MAP increased up to the basal level. The intestine and the brain responded differently to resuscitation. Intestinal blood flow significantly increased by 30±9% ($p<0.05$) reaching a level of 69% followed by a secondary decrease down to 37±11% ($p<0.01$). Blood flow in the brain increased by 26.5±8% ($p<0.01$) and stabilized at a level of 82%. The intestinal reflectance decreased sharply below its basal level, followed by an increase back to the basal levels. Cerebral reflectance showed nearly no changes except for a decrease of 12±5% ($p<0.05$) during a short period about an hour after resuscitation. Following resuscitation, NADH in both organs only partially recovered and remained elevated compared to the basal level.

When the two organs are compared during bleeding, a significant difference is observed only with respect to NADH levels ($p<0.05$). Following resuscitation, there were only two episodes of significant differences in the TBF between the organs ($p<0.05$). The TMS for the data shown were calculated. The results are presented in the fourth parameter from the top shown in Figure 24. The calculation of the index shows that during the hypotension phase the index decreased in the small intestine by 88±8%, while in the protected organ, the brain, the Index dropped only by 40±7%. The difference was significant ($p<0.01$). After the resuscitation, the recovery of the indices was not complete.

In order to understand the involvement of increase in CBF as part of the "blood flow redistribution" mechanism, we compared two groups of rats exposed to 15 minutes hemorrhage. Our hypothesis was that brain partial ischemia, may affect the protection of the brain against a decrease in oxygen supply by systemic hemorrhage. In this study, we examined the effect of partial brain ischemia on the integrity of the 'brain-sparing effect' developed under severe hemorrhage induced in the rat model, while monitoring mitochondrial NADH and microcirculatory blood flow in the brain and small intestine in real time. In our preliminary work, we found that 15 minutes of severe hemorrhage (blood pressure of 40mmHg) demonstrate clearly the "Brain Sparing Effect" [48]. Therefore, in the current study, bilateral carotid occlusion was used as a partial brain ischemia model.

Figure 25 demonstrates the responses of 9 rats to controlled hypotension, which was maintained for 15 minutes. MAP of 40 mmHg was achieved by an average withdrawal of 31±2% of the rats' total blood volume. During the hypotension phase, MAP significantly decreased (62±1mmHg, $p<0.001$). The intestine and the brain responded differently. Intestinal TBF significantly decreased (30±7%, $p<0.01$) while the brain TBF remained relatively stable, with no significant changes. Intestinal reflectance significantly increased (28±7%, $p<0.01$), while the cerebral reflectance remained stable. Intestinal NADH had two phases: an increase of 32±10% ($p<0.01$) followed by a slight decrease 10 minutes after bleeding began. Cerebral NADH increased significantly (9%±2, $p<0.01$) and was the only parameter in the brain which showed a significant response.

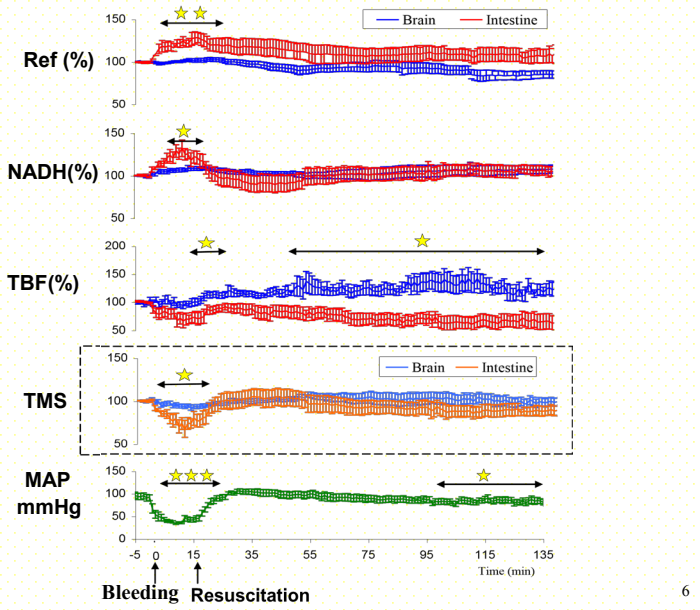

Figure 25: The responses of the brain (blue), small intestine (red) and mean arterial pressure (MAP) to controlled hypotension for 15 minutes in a group (n=9, mean ± S.E). The arrows represent the period in which significant differences were found between the two organs (in each minute) and the asterisks indicate levels of significance: *$p<0.05$, **$p<0.01$ and ***$p<0.001$. Asterisks in Ref, NADH and TBF mark significance between brain and intestine; asterisks in MAP mark significance compared to baseline. Ref - reflectance, NADH - mitochondrial NADH redox state, TBF - tissue blood flow, MAP - mean arterial pressure. Index - calculated Tissue Metabolic Score (TMS).

Following resuscitation, MAP levels fully recovered. However, about an hour after resuscitation, MAP decreased by 14±5% ($p<0.01$) until reaching significantly low levels. Following resuscitation, TBF in the intestine partially recovered reaching a level of 89±8.5%, though about 50 minutes later its levels were again signif-

icantly low following a decrease of 39±12% (p<0.01), while TBF in the brain increased by 35±11% (p<0.05). After resuscitation, intestinal reflectance decreased and gradually returned to its basal level (without significant changes). Cerebral reflectance also decreased gradually with no significant change. Intestinal NADH showed a trend of decrease below the basal level, but then it increased toward the basal value and remained steady for the rest of the experiment. Cerebral NADH decreased gradually but with no significant change, except for the resuscitation itself and several minutes afterwards when changes were significant (p<0.01).

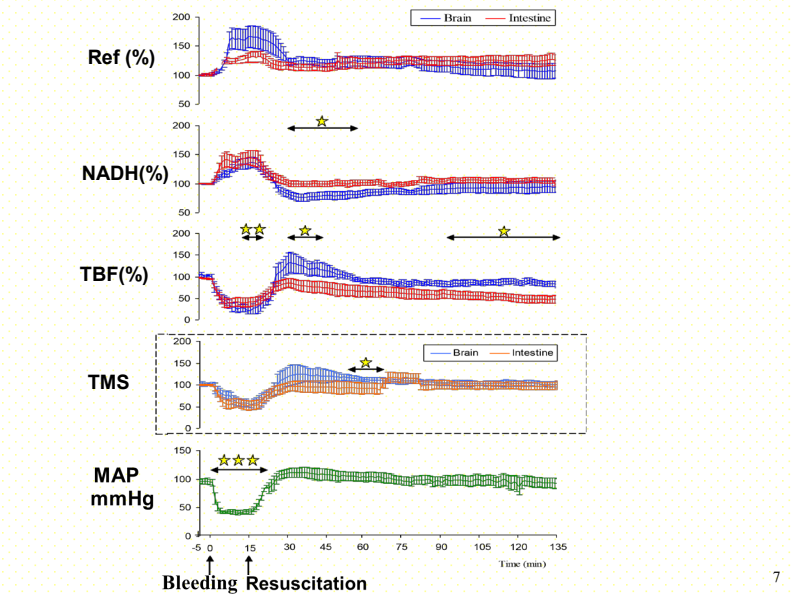

7

Figure 26: The responses of the brain (red), small intestine (blue) and mean arterial pressure (MAP) to controlled hypotension for 15 minutes following 24 hour of permanent bilateral carotid artery occlusion in a group (n=7, mean ± S.E.). The arrows represent the period in which significant differences were found between the two organs and the asterisks represent significance levels: *p<0.05, **p<0.01 and ***p<0.001. Asterisks in Ref, NADH and TBF mark significance between brain and intestine; asterisks in MAP mark significance compared to baseline. Ref - Reflectance, NADH - mitochondrial NADH redox state, TBF - tissue blood flow, MAP - mean arterial pressure. Index- calculated Tissue Metabolic Score (TMS).

In comparing the responses of the intestine and the brain during the bleeding episode, significant differences can be observed with reference to TBF (p<0.05), reflectance (p<0.01) and NADH (p<0.05). During resuscitaion, there were significant changes in the reflectance (p<0.01) and TBF (p<0.05).

In the group of ischemic rats with controlled 40 mmHg hypotension maintained for 15 minutes (24 hours following bilateral chronic carotid occlusion) only 7 rats out of 9 survived (Fig. 26). This level of hypotension was induced by bleeding out of 22%±3 of the rats' total blood volume.

As a result of the bleeding, MAP significantly decreased by 53±3.5mmHg (p<0.001). Both organs responded with a similar trend. Namely, TBF decreased rapidly and remained low for the entire hemorrhage period. Although the intestine showed a sharp decrease of 56±10% (p<0.001), the brain responded more severely by a decrease of 79.5±8% (p<0.001). Accordingly, cerebral reflectance also showed a larger increase than the intestinal reflectance (66.554±19%, p<0.05 and 30.8±9%, p<0.001 respectively). Intestinal NADH increased by 45±12% (p<0.01) whereas cerebral NADH increased by 37±9% (p<0.01). Both peaks occurred at the end of the hypotension period.

After resuscitation, MAP increased reaching the level of 112±9 mmHg (hyperemia), which was followed by a full recovery to the basal levels. Intestinal blood flow increased until reaching a level of 86±10.5% and then decreased to 46±8% (p<0.001). In contrast, the cerebral blood flow increased until reaching a level of 133±23%, then it decreased to 79±10.8% (p<0.05). Cerebral reflectance gradually decreased to the basal level. The intestinal reflectance showed a transient recovery, with a decrease and stabilization for 30 minutes followed by an elevation back to the same levels as were observed during the hypotension (133±22%). NADH in both organs fully recovered, although in a different pattern. While intestinal NADH rapidly decreased and stabilized around the basal level, cerebral NADH at first rapidly decreased below the basal levels and then fully recovered.

When comparing both organs, during the hypotension, a significant difference was observed only for the TBF ($p<0.01$). Following resuscitation, there were two episodes of significant differences in TBF, immediately after resuscitation itself and an hour later. A significant difference was also observed in NADH during the first 30 min after the resuscitation.

Testing the CritiView in Animal Models

Rats and Mongolian gerbils were used in order to test the performance of the new device as compared to laboratory devices described previously [49]. The pencil style optical probe has one measurement point to be used on exposed brain tissue (Figure 10D). The excitation and collection fibers are held together in a stainless steel element. It is comprised of one excitation fiber connected to respective excitation connector on the CritiView panel, and 6 collection fibers connected to the single collection connector on the CritiView front panel.

All experiments were performed in accordance with the Animal Care Committee of Bar-Ilan University Guidelines. The gerbil was anesthetized by an IP injection of 0.3 ml/100 gr of Equithesin (each ml contains: pentobarbital 9.72 mg; chloral hydrate 42.51 mg; magnesium sulfate 21.25 mg; propylene glycol 44.34% w/v; alcohol 11.5 % and water). During the entire experiment, the animals were maintained anesthetized. In addition, a heating pad was placed under the animal to maintain body temperature at 37°C and a rectal thermistor probe (Yellow Springs Instruments Co. Inc.) was inserted for body temperature measurements.

In the Gerbils, the two common carotid arteries were isolated just before brain surgery and ligatures of 4-0 silk thread were placed around them Figure 26. The animal was placed in a head holder in the supine position. After a midline incision of the skin, an appropriate hole was drilled in the parietal bone of the right hemisphere. The dura mater remained intact and a light guide holder – cannula was placed in the drilled hole and extra pressure on the tissue was avoided. Two stainless steel screws in the left parietal bone were used to fix the cannula, with dental acrylic cement. The gerbils were kept anesthetized during the operation as well as during the entire monitoring period, by IP injections of Eth 0.03-0.05ml every 30 minutes according to the existence of a pain response.

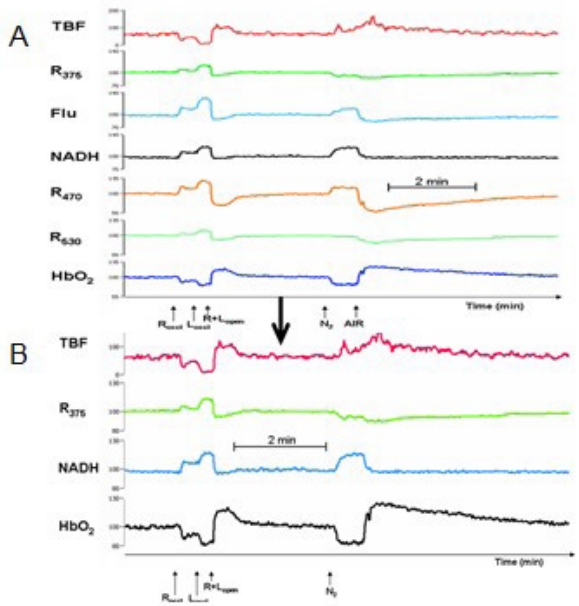

Figure 27: Monitoring of the gerbil brain by the CritiView. A - The effects of ischemia (left) and anoxia (right) on the monitored parameters measured from the brain of an anesthetized gerbil. N2 - 100% Nitrogen, Roccl, Loccl - Occlusion of the right or left common carotid artery, R+Lopen - reopening of the 2 carotid arteries. B - The 4 parameters that are extracted from the monitored parameters shown in part A.

Figure 27A presents the responses of the brain to ischemia and anoxia measured by the CritiView. Actually, the CritiView calculates data on 5 measured signals shown in part A (TBF, R_{375}, Flu, R_{470} and R_{530}) that are translated into the 4 physiological parameters, namely: TBF, R_{375}, NADH and HbO_2 (seen in part B). The

raw fluorescence signal is translated into the net NADH signal by subtracting the R_{375} from the Flu signal. The HbO_2 signal is obtained by subtracting the R_{530} (isosbestic reflectance) from the R_{470} (the non-isosbestic reflectance). The net reflectance change between the R_{470} and R_{530} is reversed in its polarity in order to demonstrate the HbO_2 in values of increase or decrease in HbO_2 and not the reflectance change. Figure 27B left side, shows the responses to complete ischemia induced by unilateral and bilateral occlusion of the carotid arteries. Due to the decrease in blood flow and volume to the brain (TBF signal) all measured signals are increasing. The net changes are a large decrease in HbO_2 correlated very well to the NADH. A small hyperemia was noticed in the TBF and HbO_2 traces. The time needed for recovery to the base line value is much shorter in the NADH signal as compared to the TBF and other reflectance signals (R_{375}, R_{470}, and R_{530}).

Under anoxia (27B right side) induced by breathing of 100% N_2 the initial response was the decrease in HbO_2 followed by an increase in NADH. The TBF showed a later increase which turned into a hyperemic response that was also recorded in the HbO_2 signal after the recovery from anoxia.

The responses to brain activation (cortical spreading depression-CSD) were recorded using the CritiView device as seen in (Figure 28). Part A shows the measured and the calculated parameters while in part B only the main 4 parameters are given. As described in section 6.2, the activation of the brain induces an increase in oxygen consumption in order to restore the ionic shift created during the CSD cycle. The black record representing the NADH redox state shows a clear oxidation (decreased signal) (Figure 28A and B). The extra oxygen needed is provided by a significant increase in cerebral blood flow (CBF) seen in the red line. The level of oxygenated hemoglobin (blue line) presents an initial increase due to the increased CBF, followed by a clear decreased due to the very large download of oxygen from the HbO_2.

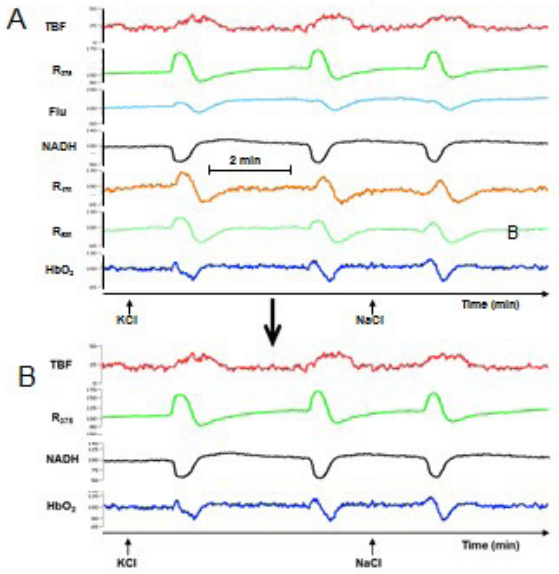

Figure 28: Monitoring of the gerbil brain by the CritiView. A - Effects of cortical spreading depression induced by epidural application of KCl. B - The 4 parameters that are extracted from the monitored parameters shown in part A.

Patients Undergoing Open Repair of Abdominal Aortic Aneurysm (AAA)

In five patients, clear but not entirely consistent responses to the clamping of the abdominal aorta were observed and recorded. During this phase of the operation, the microcirculatory blood flow in the urethra decreased in all patients, while the results of NADH measurements showed some variability. Typical responses to aortic occlusion in one of the AAA patients are shown in (Figure 29A). The preparation of the aorta for the clamping procedure (marked as A) led to a clear transient decrease in TBF, as well as an increase in the NADH level. The clamping of the aorta led to a maximal decrease in TBF in parallel to the increase in NADH. In this patient, the monitored HbO_2 showed a clear decrease during the clamping interval. Due to a decrease

in tissue blood volume, during the aortic occlusion, the reflectance trace showed a large increase until the reopening of the occluded aorta. Immediately after declamping, the initial small increase in TBF led to a fast recovery of the HbO_2 and NADH redox state. All signals recovered to the same values measured during the short control period, although the occlusion interval lasted for more than 80 minutes. Data were extracted from the 5 patients of this group according to the 6 stages of the operation: Stage 1 - 10 min before the clamp, stage 2 - 10 min after the clamp, stage 3 - mid-point of the clamping period, stage 4 - 10 min before the declamp, stage 5 - 10 min after the declamp, stage 6 – the last 5 min of monitoring in the OR. The index was calculated and presented in the 5th trace in the analog record.

The results for the 5 patients showed a pronounced decline in the mean TBF values, noted in our experiments from the second stage of the surgery up to the fourth stage (Figure 29B). The dependence of TBF on time was statistically significant. The difference was significant for all the stages of surgery (t1-t4, p=0.004), but was non-significant (p>0.05) for the partial intervals (t1-t3 and t3-t4). This analysis indicates that the only statistically significant change is between point 1 and point 4. The changes in the NADH level were significant only when the basal level (t-1) was compared to t-3. The TMS calculated for the 5 patients (green line) shows a symmetrical decrease during the occlusion and complete recovery at the end of the monitoring period.

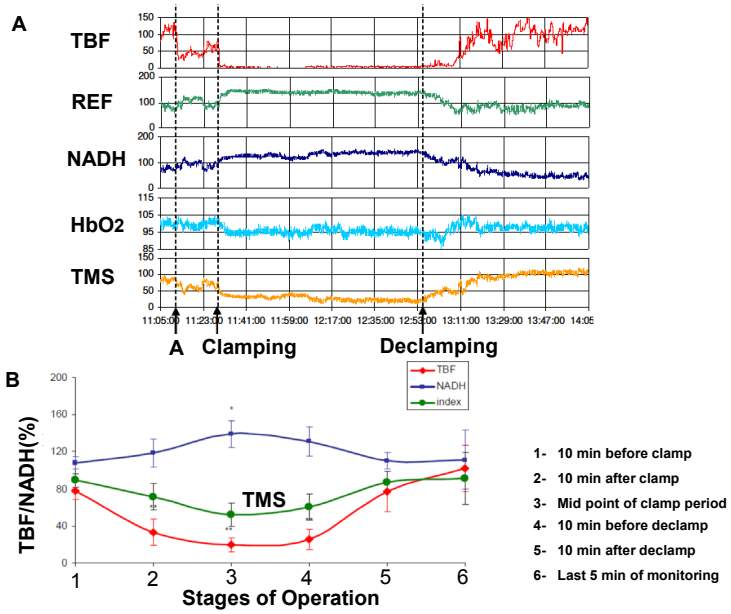

Figure 29: A - Effects of aortic occlusion in a patient that underwent an abdominal aortic aneurysm (AAA) repair operation, on the 4 parameters monitored by the CritiView. The technical preparation for aortic occlusion was performed at the marker A. Index - Tissue Metabolic Score (TMS) calculated from the monitored parameters. B-The Mean ± S.E. changes of TBF and NADH in 5 patients who underwent the AAA operation. Index - Tissue Metabolic Score (TMS) calculated from the monitored parameters (green line).

Patients Undergoing Open Heart Surgery

Thirteen patients underwent a coronary artery bypass using a cardiopulmonary bypass. Two other patients underwent an off-pump coronary artery bypass. Other two patients had valve procedures and other two underwent aortic repair using a cardiopulmonary bypass. The last patient was exposed to aortic repair as well as Coronary artery bypass grafting (CABG) procedure. Therefore 18 out of the 20 patients were operated with the use of the cardiopulmonary bypass heart-lung machine and 2 were operated under beating heart conditions. Two out of the twenty patients were exposed to deep hypothermia. Two typical responses to the cardiovascular operation procedure are presented in (Figure 30).

In the first patient shown in Figure 30A, the responses of TBF and NADH were recorded as soon as the preparation for operation started with the scrubbing of the chest area. The low level of TBF and the high level of NADH were recorded during the entire operation procedure and the recovery began as soon as the chest was closed. When the patient left the operating room for the cardiac ICU, the 2 parameters were close to the baseline levels. In the second patient operated for aortic repair, clear responses to the procedure were

recorded (Figure 30B). In this patient, the initiation of extracorporeal circulation led to a large decrease in TBF and a large increase in NADH. The signals reverted toward the initial values, although the baseline was not reached. The TMS (in green line) was calculated in the two patients and shows the dominant parameter affecting the index is the mitochondrial NADH.

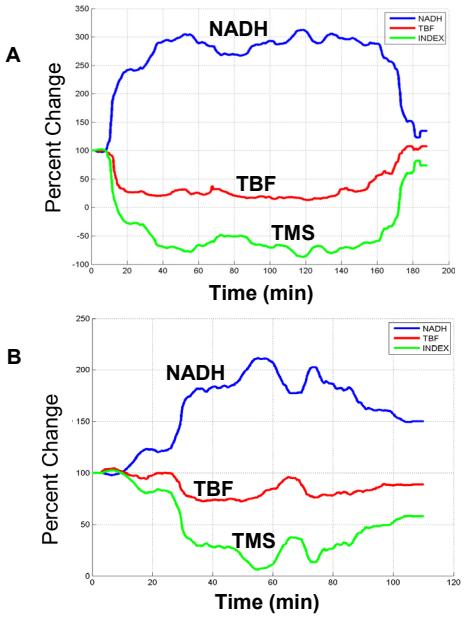

Figure 30: A - The effects of the surgical procedure, in a cardiovascular operated patient, on the urethral TBF and NADH redox state (see text for detailed explanations). Index - Tissue Metabolic Score (TMS) calculated from the monitored parameters (green line). B - The effects of the surgical procedure, in a second cardiovascular operated patient, on the urethral TBF and NADH redox state (see text for detailed explanations). Index - Tissue Metabolic Score (TMS) calculated from the monitored parameters (green line).

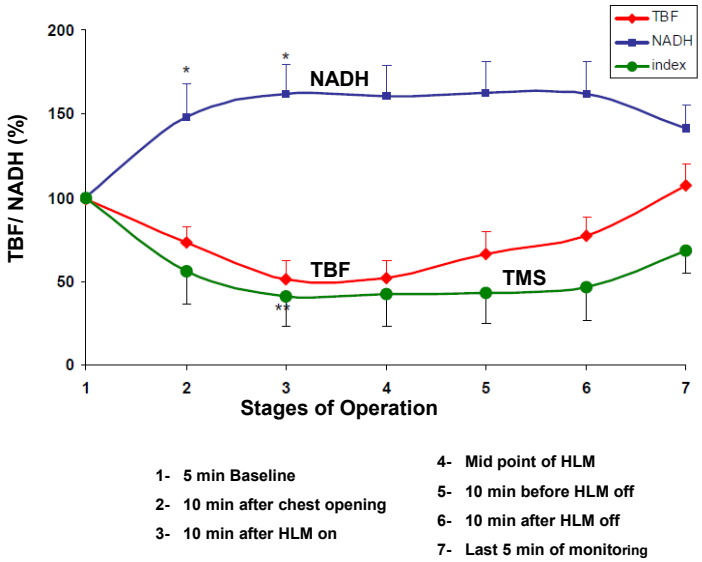

Figure 31: The Mean ± S.E. changes of TBF and NADH in 11 patients during heart bypass operation. Index - Tissue Metabolic Score (TMS) calculated from the monitored parameters (green line). See text for detailed explanation.

In order to perform statistical analysis, we selected patients that underwent a similar operation procedure. Only 13 patients were exposed to the same surgical protocol and data were extracted from 11 patients. In two patients from the CABG normothermic group, the data collection was interrupted in the middle of the operation and we were unable to calculate the results to match the other 11 patients analyzed. The other 7 patients were exposed to a different protocol and were not included in the statistical analysis. The Mean ± S.E. changes of TBF and NADH were obtained in 11 patients following heart bypass operation during 7 stages of the operation: Stage 1 - 5 min Baseline (after insertion of the catheter), Stage 2 - 10 min after chest opening,

Stage 3 - 10 min after HLM was on, Stage 4 – Mid-point of HLM, Stage 5 - 10 min before HLM was off, Stage 6 - 10 min after HLM was off, Stage 7 - the last 5 min of monitoring (Figure 31). ANOVA multiple comparison tests were conducted on the first three stages of the operation. Significance was found between point 1 and 3 in the TBF and between point 1 and points 2 and 3 in NADH (*p<0.05, ** p<0.01, n=11). The calculated index was not recovered to the baseline at the end of the monitoring period.

The next step in the patients monitoring device development will be to establish a very easy to use and practical tool, as well as to interpret the monitored parameters within the new Tissue Metabolic Score (TMS). The latter will be presented together with the 4 monitored parameters as analog signals as well as a numerical value shown in (Figure 32A and B). In one patient who underwent a routine CABG operation the same type of responses was recorded (Figure 32C). TBF reduction and NADH elevation were observed during most of the surgical procedure. Spontaneous transient recovery of TBF and NADH were noted during the second half of the operative procedure.

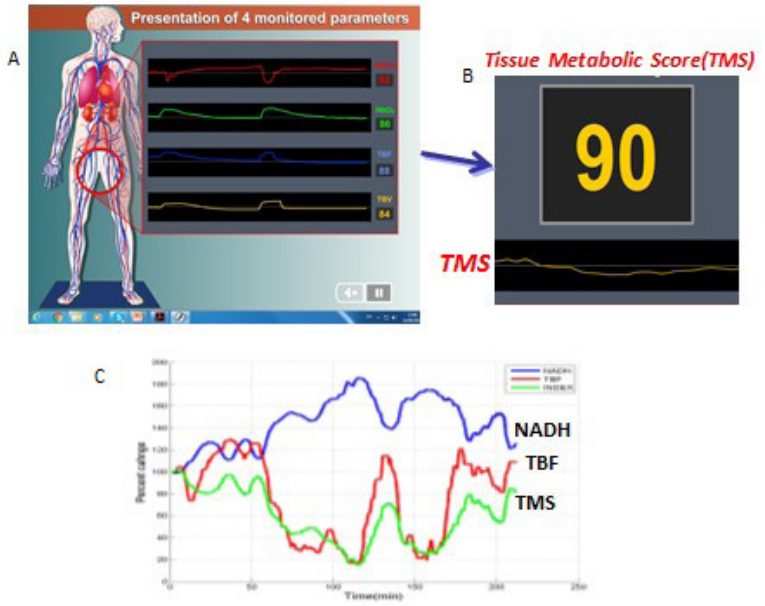

Figure 32: A - Schematic presentation of the four physiological parameters monitored in real time from the urethral wall in critical care patients. B - Schematic demonstration of the Tissue Metabolic Score (TMS) calculated from the parameters shown in Part A. C - The effects of the surgical procedure, in a third cardiovascular operated patient, on the urethral TBF and NADH redox state (see text for detailed explanations). Index - Tissue Metabolic Score (TMS) calculated from the monitored parameters (green line).

Discussion

One of the main goals in performing experiments in animal models, as well as developing new monitoring tools, is to enable the clinicians to better understand pathophysiological situations in patients as well as to develop new tools for daily use in patients. As of today, the monitoring of mitochondrial function simultaneously with microcirculatory blood flow and hemoglobin oxygenation is very rare in clinical practice. One of the main factors enabling normal tissue and organs function is the appropriate level of oxygen supply to the mitochondria needed for ATP production. The central role of mitochondrial dysfunction in various human pathological processes was established and recognized by a large number of scientists active in the field of mitochondrial function. As of today, there is a large and strong body of knowledge suggesting that the next step in patients monitoring will be to develop monitoring devices that will evaluate in real time the tissue vitality of different organs [50-52]. Although the monitoring of NADH fluorescence started during the early 1960s, the implementation of the technology into a medical device started only about 10 years ago. In this review, we present and discuss several issues that integrate some of the main topics that are critical for the future of this technology. One of the main questions to consider is: Why does the monitoring of NADH fluorescence constitute the leading technology for monitoring mitochondrial function *in vivo* and in real time? It is clear that other electron carriers in the respiratory chain may have an advantage since they are localized only in

the mitochondria. The NADH appears in addition to the mitochondria also in the cytosol and this point was discussed in previous publications [13,32]. We have tested many options that would enable us to monitor Fp fluorescence together with NADH. It was found that Fp measurement is dramatically affected by and sensitive to hemodynamic artefacts, and mainly to changes in hemoglobin oxygenation. Cytochrome oxidase monitoring suffers from the same problems due to the overlapping with hemoglobin absorption spectrum. Thus, for the near future, the NADH is the best candidate to monitor mitochondrial function in patients as well as in experimental animals.

From Isolated Mitochondria to Clinical Monitoring of NADH

The pioneering works of Chance, Williams, Connelly and other collaborators, in the early 1950s, created new possibilities enabling the study of mitochondrial function *in vitro*, and later on *in vivo* monitoring became a reality [53,54]. The shift from studying mitochondrial NADH redox state in isolated mitochondria to higher cellular and tissue organization levels started in the late 1950s [55]. The main breakthrough occurred in 1962, a year when at least 6 papers described the *in vivo* monitoring of various organs in the anesthetized rat [11,56].

After more than 60 years of monitoring of NADH fluorescence in many biological systems, two issues require the researchers' special attention:
1. Can we extrapolate from the results obtained in monitoring mitochondrial NADH *in vitro* to *in vivo* conditions?
2. Can we compare the results obtained in animal models to events developed in patients?

Mitochondrial function and its metabolic states under *in vivo* conditions are completely different from the definitions made for isolated mitochondria by Chance and Williams in 1955. The main differences between the two situations are as follows:
1. The isolated mitochondria are not inter-connected to other intracellular organelles and components.
2. The amount of oxygen available in the mitochondrial medium is not regulated by changes in blood flow or hemoglobin oxygenation under *in vitro* conditions.
3. Several of the largest oxygen or energy consumers, i.e. various ions pumps, are lacking in the isolated mitochondria preparation.
4. When ADP is added to State 4 mitochondria, ATP will be synthesized but will not be consumed in parallel, as it occurs under *in vivo* conditions.
5. The isolated mitochondria preparation is not exposed to systemic changes in hemodynamic and other physiological parameters occurring in the organism.

Since 1962 a very large number of papers described the use of NADH monitoring in intact animals exposed to a variety of physiological and pathological conditions. NADH was monitored in various animal models exposing most of the organs in the body to various perturbations [4,57].

From Single Parameters to the Multiparametric Monitoring Approach

In order to understand the changes in NADH measured *in vivo*, it was necessary to move from a single parameter monitoring to the multiparametric approach. As described in Figure 4, the NADH represents also the balance between oxygen consumption and supply. Therefore, the multiparametric approach provides a better understanding of the pathophysiological processes developed. Thus, by using 2 parameters, namely CBF and NADH, the clinician will be able to diagnose the pathological state developed as compared to a single parameter monitoring. For example, when the brain is exposed to hypoxia, the NADH increases together with an increase in CBF, due to the compensation process in the brain. But when the brain is exposed to ischemia, the NADH increases, while CBF decreases. Therefore, it would be difficult to differentiate between hypoxia and ischemia in the brain if we measured only the NADH. Another example is the correlation between 3 of the monitored parameters shown in Figure 4, namely NADH, tissue blood flow and Hb oxygenation.

The correlation between the responses of the three monitored parameters to various perturbations is not identical. For example, under ischemia, the CBF and HbO_2 are decreased, while NADH in the brain is elevated. In hypoxia, CBF is elevated in order to provide more oxygen in response to the decrease in the oxygenation of the blood, but NADH is elevated. In hyperoxia, induced by hyperbaric oxygenation, the relationship between the three parameters is different. Although the blood flow decreases, due to vasoconstriction, the NADH becomes more oxidized due to the increased oxygen supply by the higher level of oxygen in the blood plasma and the elevated HbO_2 saturation in the microcirculation. In our clinical monitoring device, we are able to monitor 4 parameters utilizing the optical approach and provide information regarding the mitochondrial NADH together with microcirculatory blood flow, volume and hemoglobin oxygenation.

Disclosure

Avraham Mayevsky was one of the founders of CritiSense Ltd. that had developed the CritiView device presented in the current manuscript. He was one of the shareholders and served as a director in the BOD. He received consultation fees from the company during the company activity (2004-2007), while serving as chief scientist. The company was closed in 2017.

Conclusions

The new approach to monitor patients in emergency rooms and ICUs, by the CritiView, was tested successfully under *in vitro* and animal *in vivo* experiments as well as in patients. The conclusions from this study are the following:

a. For the first time, mitochondrial NADH, microcirculatory blood flow and hemoglobin oxygenation were measured continuously in the urethral wall of patients.

b. Patients exposed to vascular and open chest surgeries showed changes in the urethral wall measured parameters during stressful conditions of the body.

c. The CritiView results may serve as early warning signals for the deterioration of the body or the end point of resuscitation during and after cardiovascular surgeries.

d. The developed Tissue Metabolic Score (TMS) should be tested in a large-scale clinical study.

The crucial questions that remains open:

1. Could we interpret the *in vivo* data according to the concepts developed for *in vitro* conditions?
2. Can we compare and define the resting state (4) and active state (3) under *in vivo* situations to the *in vitro* definitions?
3. How can we overcome the issue of the missing technique for the calibration of NADH signal monitoring *in vivo* in absolute values?

References

1. Chance B, Oshino N, Sugano T, Mayevsky A (1973) Basic principles of tissue oxygen determination from mitochondrial signals. Oxygen Transport to Tissue, Adv Exp Med Biol 37A: 277-92.

2. Altmann R (1890) Die Elementarorganismen Und Ihre Beziehungen Zu Den Zellen, Veit & comp, Leipzig, Germany.

3. Benda C (1898) Ueber die Spermatogenese der Vertebraten und höherer Evertebraten, II. Theil: Die Histiogenese der Spermien. Arch Anat Physiol 73: 393-8.

4. Mayevsky A, Barbiro-Michaely E (2013) Shedding light on mitochondrial function by real time monitoring of NADH fluorescence: I. Basic methodology and animal studies. J Clin Monit Comp 27: 1-34.

5. Warburg OH, Dickens F (1930) Metabolism of Tumors, Constable & Co. Ltd, London.

6. Modica-Napolitano JS, Kulawiec M, Singh KK (2007) Mitochondria and human cancer. Curr Mol Med 7: 121-31.

7. Ying W (2007) NAD+ and NADH in brain functions, brain diseases and brain aging. Front Biosci 12: 1863-88.

8. Edeas M, Weissig V (2013) Targeting mitochondria: Strategies, innovations and challenges The future of medicine will come through mitochondria. Mitochondrion 13: 389-90.

9. Harden A, Young W (1906) Alcoholic ferment of yeast-juice Part II Co-ferment of yeast-juice. Proc Roy Soc B78: 369-75.

10. Warburg O, Christian W, Griese A (1935) Wasserstoff-Ubertragendes Co-ferment, seine Zusamensetzung und Wirkungsweise. Biochem Zeitschrift 282: 157.

11. Chance B, Cohen P, Jobsis F, Schoener B (1962) Intracellular oxidation-reduction states in vivo. Science 137: 499-508.

12. Kohen E, Kohen C, Thorell B (1969) Use of microfluorimetry to study the metabolism of intact cells. Biomed Eng 4: 554-9.

13. Mayevsky A (1984) Brain NADH redox state monitored in vivo by fiber optic surface fluorometry. Brain Res Rev 7: 49-68.

14. Chance B, Williams GR (1955) Respiratory enzymes in oxidative phosphorylation (III- The steady state). J Biol Chem 217: 409-27.

15. Barcroft J (1914) The Respiratory Function of Blood, Cambridge University Press, Cambridge, UK.

16. Mayevsky A, Doron A, Manor T, Meilin S, Zarchin N, et al. (1996) Cortical spreading depression recorded from the human brain using a multiparametric monitoring system. Brain Res 740: 268-74.

17. Mayevsky A, Nakache R, Merhav H, Luger-Hamer M, Sonn J (2000) Real time monitoring of intraoperative allograft vitality. Transplant Proc 32: 684-5.

18. Mayevsky A, Nakache R, Luger-Hamer M, Amran D, Sonn J (2001) Assessment of transplanted kidney vitality by a multiparametric monitoring system. Transplant Proc.33: 2933-4.

19. Vici P, Pizzuti L, Gamucci T, Sergi D, Conti F, et al. (2014) Non-pegylated liposomal doxorubicin-cyclophosphamide in sequential regimens with taxanes as neoadjuvant chemotherapy in breast cancer patients. J Cancer 5: 398-405.

20. Mayevsky A, Deutsch A, Dekel N, Pevzner E, Jaronkin A (2005) A new biomedical device for in vivo multiparametric evaluation of tissue vitality in critical care medicine. Proc SPIE 5692: 60-70.

21. Mayevsky A, Blum Y, Dekel N, Deutsch A, Halfon R, et al. (2006) The CritiView - A new fiber optic based optical device for the assessment of tissue vitality. Proc SPIE 6083: 0Z-1-0Z-9.

22. Mayevsky A, Dekel N, Oren L, Deutsch A, Pewzner E (2008) Mitochondrial dysfunction: bench-to-bedside optical monitoring of tissue vitality. In: Mahadevan-Jansen A, Petrich W, Alfano RR, Katz A, editors. Biomedical Optics (BiOS) 2008, International Society for Optics and Photonics 68531B-11.

23. Hotchkiss RS, Karl IE (1992) Reevaluation of the role of cellular hypoxia and bioenergetic failure in sepsis. JAMA 267: 1503-10.

24. Marik PE, Varon J (1998) The hemodynamic derangements in sepsis: implications for treatment strategies. Chest 114: 854-60.

25. Ince C, Sinaasappel M (1999) Microcirculatory oxygenation and shunting in sepsis and shock. Crit Care Med 27: 1369-77.

26. Meier-Hellmann A, Reinhart K (1995) Effects of catecholamines on regional perfusion and oxygenation in critically ill patients. Acta Anaesthesiol Scand Suppl 107: 239-48.

27. Ekbal NJ, Dyson A, Black C, Singer M (2013) Monitoring tissue perfusion, oxygenation, and metabolism in critically ill patients. Chest 143: 1799-808.

28. Fullerton JN, Singer M (2011) Organ failure in the ICU: cellular alterations. Semin Respir Crit Care Med 32: 581-6.

29. Mayevsky A (1992) Cerebral blood flow and brain mitochondrial redox state responses to various perturbations in gerbils. Adv Exp Med Biol 317: 707-16.`

30. Manor T, Barbiro-Michaely E, Rogatsky G, Mayevsky A (2008) Real-time multi-site multi-parametric monitoring of rat brain subjected to traumatic brain injury. Neurol Res 30: 1075-83.

31. Barbiro-Michaely E, Tolmasov M, Rinkevich-Shop S, Sonn J, Mayevsky A (2007) Can the "brain-sparing effect" be detected in a small-animal model? Med Sci Monit 13: Br211-9.

32. Mayevsky A, Rogatsky GG (2007) Mitochondrial function in vivo evaluated by NADH fluorescence: From animal models to human studies. Am J Physiol Cell Physiol 292: C615-C40.

33. Ince C, Coremans JMCC, Bruining HA (1992) In vivo NADH fluorescence. In: Erdmann W, Bruley DF, editors., Adv Exp Med Biol.Vol 317, Plenum Press, New York, USA.

34. Bradley RS, Thorniley MS (2005) A review of attenuation correction techniques for tissue fluorescence. J Royal Soc Interface 3: 1-13.

35. Mayevsky A, Manor T, Pevzner E, Deutsch A, Etziony R, et al. (2004) Tissue spectroscope: a novel in vivo approach to real time monitoring of tissue vitality. J Biomed Opt 9: 1028-45.

36. Pevzner, E., Deutsch, A., Manor, T., Dekel, N., Etziony, R., Derzy, I., Razon, N. and Mayevsky, A. (2003) Real-time multiparametric spectroscopy as a practical tool for evaluation of tissue vitality in vivo. In: Advances Biomedical and Clinical Diagnostic Systems, Proc. SPIE, vol. 4958, Eds. T. Vo-Dinh, W.S. Grundfest, D.A. Benaron and G.G. Cohn, pp. 171-82.

37. Mayevsky A, Barbiro-Micahely E, Kutai-Asis H, Deutsch A, Jaronkin A (2004) Brain physiological state evaluated by real time multiparametric tissue spectroscopy in vivo. Proc SPIE 5326: 98-105.

38. Mayevsky A, Sonn J, Barbiro-Michaely E (2013) Physiological mapping of brain functions in vivo: Surface monitoring of hemodynamic metabolic ionic and electrical activities in real-time. J Neurosci Neuroeng 2: 150-77.

39. Mayevsky A, Preisman S, Willenz PE, Castel D, Perel A, et al. (2009) Evaluation of the CritiView in a pig model of abdominal aortic occlusion and graded hemorrhage. SPIE Proc 7173: OL1-10.

40. Mayevsky A, Walden R, Pewzner E, Deutsch A, Heldenberg E, et al. (2011) Mitochondrial function and tissue vitality: bench-to-bedside real-time optical monitoring system. J Biomed Opt 16: 067004.

41. Mayevsky A, Chance B (1973) A new long-term method for the measurement of NADH fluorescence in intact rat brain with implanted cannula. Adv Exp Med Biol 37A: 239-44.

42. Leao AAP (1944) Spreading depression of activity in cerebral cortex. J Neurophysiol 7: 359-90.

43. Leao AAP (1944) Pial circulation and spreading depression of activity in the cerebral cortex. J Neurophysiol. 7: 391-6.

44. Mayevsky A, Weiss HR (1991) Cerebral blood flow and oxygen consumption in cortical spreading depression. J Cereb Blood Flow Metab 11: 829-36.

45.Waltemath CL (1970) Oxygen, uptake, transport, and tissue utilization. Anesth Analg. 49: 184-203.

46. Schnitge.H, Scholz R, Bucher T, Lubbers DW (1965) Comparative fluorometric studies on rat liver in vivo and on isolated, perfused hemoglobin free liver Biochem Z 341: 334.

47. Mayevsky A, Lebourdais S, Chance B (1980) The interrelation between brain PO2 and NADH oxidation- reduction state in the gerbil. J Neurosci Res 5: 173-82.

48. Mandelbaum MM, Barbiro-Michaely E, Tolmasov M, Mayevsky A (2008) Effects of severe hemorrhage on in vivo brain and small intestine mitochondrial NADH and microcirculatory blood flow. J Innov Opt Health Sci 01: 177-83.

49. Meirovithz E, Sonn J, Mayevsky A (2007) Effect of hyperbaric oxygenation on brain hemodynamics, hemoglobin oxygenation and mitochondrial NADH. Brain Res Rev 54: 294-304.

50. Harrois A, Dupic L, Duranteau J (2011) Targeting the microcirculation in resuscitation of acutely unwell patients. Curr Opin Crit Care 17: 303-7.

51. Chance B, Nioka S, Warren W, Yurtsever G (2005) Mitochondrial NADH as the bellwether of tissue O2 delivery. Adv Exp Med Biol 566: 231-42.

52. Singer M (2007) Mitochondrial function in sepsis: acute phase versus multiple organ failure. Crit Care Med 35: S441-8..

53. Chance B, Williams GR (1956) The respiratory chain and oxidative phosphorylation. In: Nord FF, editor. Advances in Enzymology, Interscience Publisher 17: 65-134.

54. Connelly CM, Chance B (1954) Kinetics of reduced pyridine nucleotides in stimulated frog muscle and nerve. Am Physiol Soc 13: 29.

55. Chance B, Jobsis F (1959) Changes in fluorescence in a frog sartorius muscle following a twitch. Nature 184: 195-6.

56. Chance B, Legallias V, Schoener B (1962) Metabolically linked changes in fluorescence emission spectra of cortex of rat brain, kidney and adrenal gland. Nature 195: 1073-5.

57. Mayevsky A, Barbiro-Michaely E (2013) Shedding light on mitochondrial function by real time monitoring of NADH fluorescence: II: Human studies. J Clin Monit Comp 27: 125-45.